

Simulation study of wave phenomena from the sheath region in single frequency capacitively coupled plasma discharges; field reversals and ion reflection

S. Sharma^{a)} and M. M. Turner

*National Centre for Plasma Science and Technology, School of Physical Sciences,
Dublin City University, Dublin 9, Ireland*

(Dated: 28 June 2013)

Capacitively coupled radio-frequency discharges have great significance for industrial applications. Collisionless electron heating in such discharges is important, and sometimes is the dominant mechanism. This heating is usually understood to originate in a stochastic interaction between electrons and the electric fields. However, other mechanisms may also be important. There is evidence of wave emission with a frequency near the electron plasma frequency, *i.e.* ω_{pe} , from the sheath region in collisionless capacitive radio-frequency (RF) discharges. This is the result of a progressive breakdown of quasi-neutrality close to the electron sheath edge. These waves are damped in a few centimeters during their propagation from the sheath towards the bulk plasma. The damping occurs because of the Landau damping or some related mechanism. This research work reports that the emission of waves is associated with a field reversal during the expanding phase of the sheath. Trapping of electrons near to this field reversal region is observed. The amplitude of the wave increases with increasing RF current density amplitude \tilde{J}_0 until some maximum is reached, beyond which the wave diminishes and a new regime appears. In this new regime, the density of the bulk plasma suddenly increases because of ion reflection which occurs due to presence of strong field reversal near sheath region. Our calculation shows that these waves are electron plasma waves. These phenomena occur under extreme conditions (*i.e.* higher \tilde{J}_0 than in typical experiments) for sinusoidal current waveforms, but similar effects may occur with non-sinusoidal pulsed waveforms for conditions of experimental interest, because the rate of change of current is a relevant parameter. The effect of electron elastic collisions on plasma waves is also investigated.

PACS numbers: 52.25.Mq, 52.25.-b, 52.70.Gw

^{a)}Corresponding author:sarvsarvesh@gmail.com

I. INTRODUCTION

Wave-particle interaction plays an important role in the physics of ionized matter. The nature of this complex interaction in plasmas has predominantly been studied by analytical and simulation methods¹⁻³. Recently, experimental investigations have also been possible due to advances in optical diagnostics with high temporal resolution⁴⁻⁹. There is an evidence of electron plasma wave propagation from the sheath edge towards the bulk plasma in the literature^{10,11,23}, although no relevant theory is proposed and no detailed analysis of their nature has yet been given. When the sheath expands, quasi-neutrality breaks down due to an overshoot of high velocity electrons into the bulk plasma. Due to this, electron plasma waves are emitted from the sheath region. The electrons interact strongly with the oscillating potential and on an average gain energy through nonlinear wave-particle interactions. An approach based on quasi-linear theory which attempts to link stochastic heating with collisionless power dissipation through wave-particle interaction has appeared in the literature^{24,25}. There are several attempts in the literature which link the capacitive collisionless heating effects with acoustic or plasma wave phenomena²⁷⁻³⁰, but none of these efforts have yet produced a generally satisfying treatment. However it is certainly possible for the oscillating energy to be transferred to electron thermal energy by the well-known mechanism of Landau damping³¹ or a related process. Landau damping occurs due to the energy exchange between a wave with phase velocity $v_{ph} = \omega/k$ and particles in the plasma with velocity approximately equal to v_{ph} , which can interact strongly with the wave. Here k is a wave vector. Those particles having velocities slightly less than v_{ph} will be accelerated by the wave electric field to move with the wave phase velocity, while particles with velocities slightly greater than v_{ph} will be decelerated by the wave electric field, losing energy to the wave. Power dissipation through wave-particle interaction in capacitively coupled plasmas (CCPs) has been predicted in particle-in-cell (PIC) simulation by Vender and Boswell¹¹. Later Gozadinos et al.¹⁰ also reported oscillations near the sheath vicinity in PIC simulation. These effects are clearly dependent on the excitation intensity of the sheath, and this is usefully characterized for sinusoidal waveforms by the parameter H , defined by Lieberman¹² as

$$H = \frac{\tilde{J}_0^2}{\pi \epsilon_0 k_B T_e \omega_r^2 n_{sm}}, \quad (1)$$

where T_e is the electron temperature, n_{sm} is the plasma density at the sheath edge, and ω_{rf} is the angular excitation frequency. In most experiments but not all $H \sim 5$ and these effects are not observed. Recently, it is reported that the power deposition in CCPs discharges can be enhanced by replacing sinusoidal waveforms with non-sinusoidal waveforms *e.g.* Gaussian shaped voltage pulses³⁹. In this work the authors used a particle-in-cell (PIC) simulation and showed that the electron heating can be directly controlled by changing the Gaussian pulse width. Later Lafleur et al.⁴⁰ used pulse-type tailored waveforms in argon plasma experiments in a geometrically symmetric CCP discharges and confirmed a number of predictions made by PIC simulations of a similar system³⁹. In a concluding remark, the phenomena under discussion in the present research work occur under extreme conditions *i.e.* at high \tilde{J}_0 or H for sinusoidal waveforms, but for non-sinusoidal pulsed waveforms the strong wave phenomena and new regime appear under less extreme conditions. So the present research work has a possible practical relevance. The detailed investigation of these waves in the case of sinusoidal discharges is the main aim of present research work.

In this paper, we first present the analytical single frequency heating model in Sec. II. We try to understand the wave phenomena, presence of field reversal and electron trapping effect in single frequency RF discharges with the help of Particle-in-Cell simulation in half-infinite plasma in Sec. III. The effect of electron elastic collisions with neutrals on waves is discussed in Sec. IV. Finally we summarize our conclusions and discuss the results in Sec. V.

II. ANALYTICAL SINGLE FREQUENCY MODELS

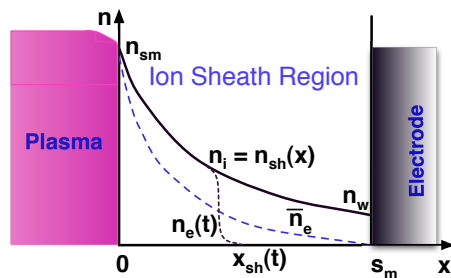


FIG. 1. Schematic diagram of the densities in a high voltage capacitive RF sheath.

Low pressure discharges are sustained by radio-frequency (RF) currents and voltages ap-

plied directly to an electrode immersed in the plasma. A high voltage capacitive sheath then forms between the electrode and the bulk plasma. At low pressure, ohmic heating is not the main source of power absorption and electrons gain energy by interacting with the high voltage oscillating sheath. This heating mechanism is called stochastic or collisionless heating. Stochastic heating has been studied using different models^{12-17,27} as well as experiments¹⁸⁻²². The calculation of stochastic heating for a collisionless nonuniform high voltage RF sheath has been discussed by Lieberman¹². The structure of the RF sheath is shown in figure 1. Ions cross the ion sheath boundary at $x = 0$ with a velocity of the order of the Bohm speed $u_B = (k_B T_e / m_i)^{1/2}$, are further accelerated within the sheath by the sheath potential, and finally strike the electrode at $x = s_m$ with high energies. The ion motion is collisionless here. Since the ion velocity increases as it approaches the electrode, due to ion flux conservation, the ion density $n_{sh}(x)$ decreases continuously from its maximum value n_{sm} (at the ion-sheath plasma boundary) to its minimum value n_w (at the electrode, as in figure 1). So in a self-consistent discharge, the plasma density is not uniform. In figure 1, $x_{sh}(t)$ is the instantaneous position of the oscillating electron sheath edge. The electron sheath edge oscillates between the wall at $x = s_m$ and the ion sheath boundary at $x = 0$. A self-consistent analysis of the dynamics of a high voltage collisionless capacitive RF sheath is given by Lieberman¹². A positive net power deposition has also been obtained by Lieberman¹² for a collisionless RF sheath driven by a sinusoidal current $J_{rf}(t) = \tilde{J}_0 \sin \omega_{rf} t$, given by

$$S_{stocL} = \frac{3\pi}{32} H m_e n_{sm} \bar{v}_e u_0^2 \quad (2)$$

where $\bar{v}_e = [8k_B T_e / (\pi m_e)]^{1/2}$ is the mean electron thermal velocity, u_0 is the drift velocity at the ion sheath edge and H is the control parameter defined above. Waves occurring near to the sheath region may contribute to the stochastic heating phenomena, but such effects are not captured by eq. 2.

III. SIMULATION RESULTS OF HALF-INFINITE PLASMA

In this work, a self-consistent semi-infinite particle-in-cell (PIC) method is used for current-driven argon discharges in which both the electrons and ions were moved by conventional PIC methods. This procedure simulates a finite region at the edge of a semi-infinite plasma, characterized by a given density (n_{sm}) and electron temperature (T_e). Ions enter

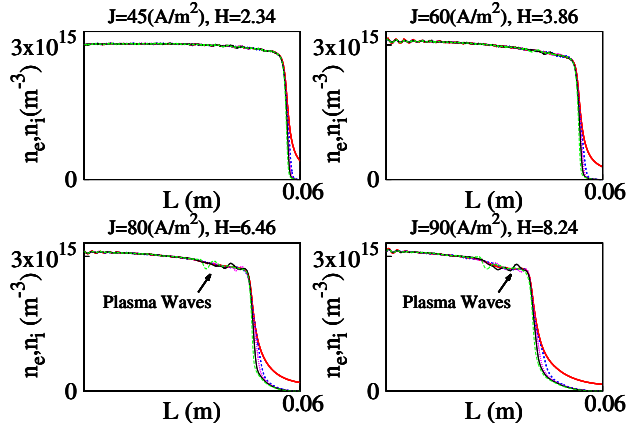


FIG. 2. Snapshots of ion and electron density profile in PIC simulation. The solid line (red) represents the average ion density and electron density is represented by lines at different times during an RF period *i.e.* $t = 0.244 T_{rf}$ (blue), $t = 0.283 T_{rf}$ (magenta), $t = 0.322 T_{rf}$ (black) and $t = 0.38 T_{rf}$ (green). Conditions : $\tilde{J}_0 = 45 - 90 \text{ A/m}^2$, $f_{rf} = 27.12 \text{ MHz}$, $H \approx 2.34 - 8.24$, $T_e = 2.5 \text{ eV}$, $T_i = 0.03 \text{ eV}$, argon plasma density = $3.0 \times 10^{15} \text{ m}^{-3}$.

the simulation at one wall with a drift velocity equal to the Bohm speed, u_B , and electrons are injected with drifting Maxwellian distribution functions in a manner consistent with the boundary conditions. A second boundary represents an electrode driven by a radio-frequency current. Simulation particles that reach either boundary are absorbed. This procedure is described in detail in the literature³². These results are for the collisionless case so electron and ion collisions are not included. In effect, we assume that the mean free paths of the charged particles are larger than the size of the simulation region. In argon, for example, this implies a pressure of 10 mTorr or less.

We note that, strictly speaking, the boundary condition that we impose is on the ion flux entering the simulation region³². When the ions enter with a given speed and are collisionless, under ordinary conditions this is entirely equivalent to specifying the plasma density, n_{sm} . However, when ions are reflected from the sheath, as happens in certain cases discussed below, then this equivalence does not hold, and the plasma density at the boundary does not depend only on the injected flux. Under this extraordinary condition, the plasma density may vary with the RF current density, as we describe below.

These PIC simulations are for the case where the applied frequency f_{rf} is 27.12 MHz and system length l is 0.06–0.105 m. The electron temperature T_e is 2.5 eV and ion temperature

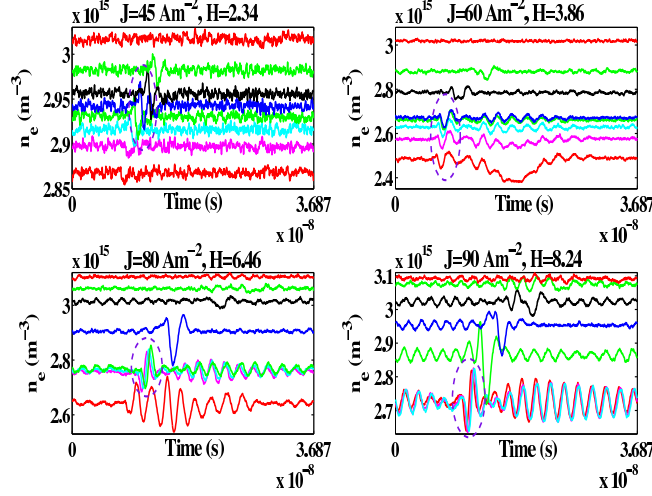


FIG. 3. Temporal evolution of electron plasma waves in electron density profile. Here the electron density is plotted at the different positions of the system length for an RF period. For $\tilde{J}_0 = 45$ A/m², the wave starts near sheath region at 5.09 cm (bottom red line) propagate towards bulk plasma and clearly visible at 4.51 cm (blue line) and finally disappear near 2.93 cm (top red line). For $\tilde{J}_0 = 60$ A/m², the wave starts near sheath at 5.3 cm (bottom red line) propagate towards bulk and finally disappear at 2.93 cm (top red line). For $\tilde{J}_0 = 80$ A/m², the wave starts at 4.69 cm (bottom red line) propagate towards bulk and clearly visible near 4.34 cm (magenta) and disappear at 0.88 cm (top red line). Finally for $\tilde{J}_0 = 90$ A/m² the wave appear at 3.98 cm (bottom red line) propagate and disappear near 0.59 cm (top red line). Conditions : $\tilde{J}_0 = 45 - 90$ A/m², $f_{rf} = 27.12$ MHz, $H \approx 2.34 - 8.24$, $T_e = 2.5$ eV, $T_i = 0.03$ eV at argon plasma density = 3.0×10^{15} m⁻³.

T_i is 0.03 eV for all sets of simulation here. This ion temperature has little influence on the simulation results. The *RF* current drive amplitude $\tilde{J}_0 = 45 - 90$ A/m² is applied at density = 3×10^{15} m⁻³.

Figure 2 shows the averaged ion and snapshots of the electron density profile for $\tilde{J}_0 = 45 - 90$ A/m² and $H \approx 2.34 - 8.24$ at different times during an *RF* period. As shown in figure 2, the ion density $n_{sh}(x)$ decreases monotonically from maximum density at the ion sheath boundary to a minimum of $n_w = 4.1 \times 10^{14}$ m⁻³, 2.85×10^{14} m⁻³, 1.89×10^{14} m⁻³ and 1.488×10^{14} m⁻³ at the wall (electrode) for corresponding $\tilde{J}_0 = 45 - 90$ A/m² respectively. The interesting phenomena can be observed on the right side of the figure, when the electron sheath expands (dashed lines) and the traveling oscillations occur near to the sheath edge. These travel-ing oscillations propagate towards the bulk plasma. The following conclusions

can be made from figure 2: (i) Sheath width increases with increasing \tilde{J}_0 or H (ii) Electron plasma waves are absent at lower values of \tilde{J}_0 or H (iii) Electron plasma waves appear at

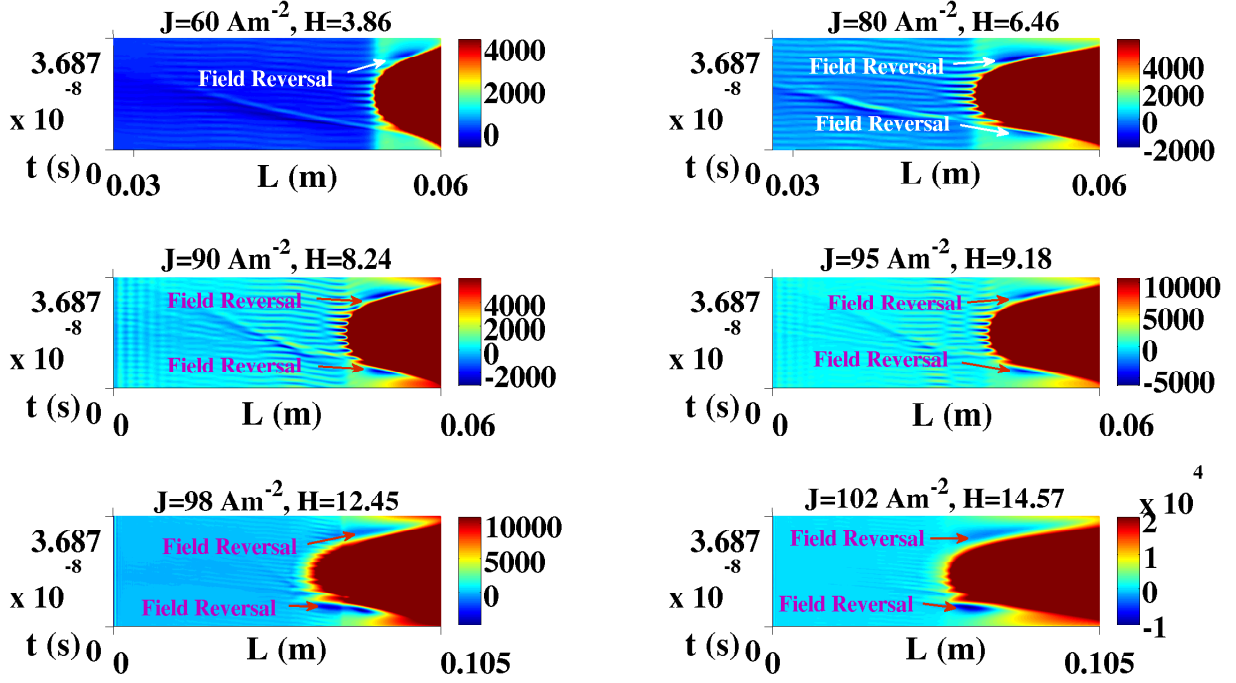


FIG. 4. Spatiotemporal profile of electric field for different values of H . This figure shows the very high electric field inside the sheath and weak field in the bulk plasma. The field reversal region can be observed during the sheath expansion (for higher H) and when the sheath retreats towards electrode (for all H). Conditions : $\tilde{J}_0 = 60 - 102 \text{ A/m}^2$, $f_{rf} = 27.12 \text{ MHz}$, $H \approx 3.86 - 14.57$, $T_e = 2.5 \text{ eV}$, $T_i = 0.03 \text{ eV}$ at argon plasma density = $3.0 \times 10^{15} \text{ m}^{-3}$.

Figure 3 shows the temporal evolution of electron density (n_e), for the initial conditions shown in figure 2. This temporal evolution suggests the following points: (i) waves are present in each case *i.e.* from $H = 2.34 - 8.24$; (ii) for lower values of H , the wave amplitude is weak and the waves are not discernible in the spatial profile of the electron density; (iii) the wave amplitude increases with increasing H and at higher H , the wave amplitude is significant and is clearly apparent in the spatial profile of the electron density; (iv) the electron plasma waves propagate towards the bulk plasma and finally disappear after a few centimeters.

It is important to investigate the reason behind for the origin of these waves. Figure 4 shows the spatiotemporal profile of the electric field. Here H is varying from $3.86 - 14.57$ for

the corresponding \tilde{J}_0 from 60 – 102 A/m². When the sheath collapses, a field reversal region

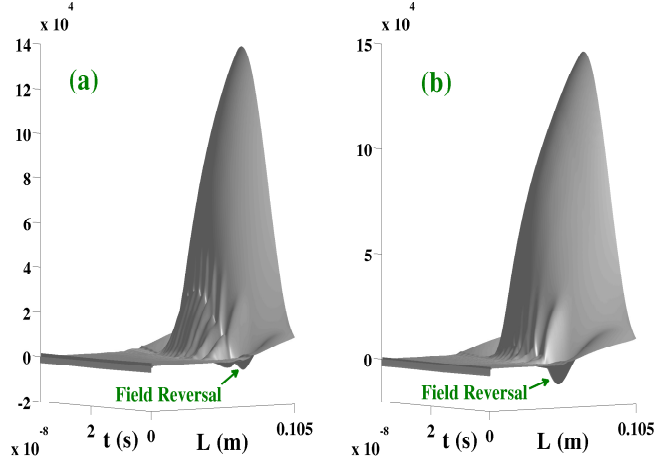


FIG. 5. A surface plot of electric field which indicates a strong field reversal during the sheath expansion. (a) For $\tilde{J}_0 = 98$ A/m² (b) For $\tilde{J}_0 = 102$ A/m². Conditions: $T_e = 2.5$ eV, $T_i = 0.03$ eV, $f_{rf} = 27.12$ MHz at argon plasma density = 3.0×10^{15} m⁻³.

appears near the sheath edge in each case. For hydrogen and electronegative plasmas, field reversal has been reported in the literature^{33–37}. Field reversal is also reported for the case of rare gas discharges (neon)^{8,9}. The origin of the field reversal during the collapsing phase of sheath is straightforward and discussed in the literature⁸. The electrons are accelerated with the sheath edge as the sheath collapses towards the electrode. However, the thermal velocity of electrons is finite and does not allow them to simply diffuse with the collapsing sheath. Because of this a local region of space charge comes into play, called field reversal, which accelerates electrons towards the electrode.

The most interesting part, which is not reported yet in the literature, is the presence of field reversal during the expanding phase of the sheath. Most researchers work with low values of H and the existence of the strong field reversal at the time of sheath expansion is not observed there. It is important to note that at higher values of H (> 9), the field reversal during the expanding phase of the sheath is several times higher than the field reversal during the collapsing phase of the sheath. Figure 5 shows the surface plot of electric field for $H = 12.45$ ($\tilde{J}_0 = 98$ A/m²) and 14.57 ($\tilde{J}_0 = 102$ A/m²). The most probable reason for this field reversal is the electron fluid compression and rarefaction while the sheath expands and collapses. Physically, this phenomena can be understood as follows. When electrons move from the bulk towards the sheath; high energy electrons first feel the high sheath

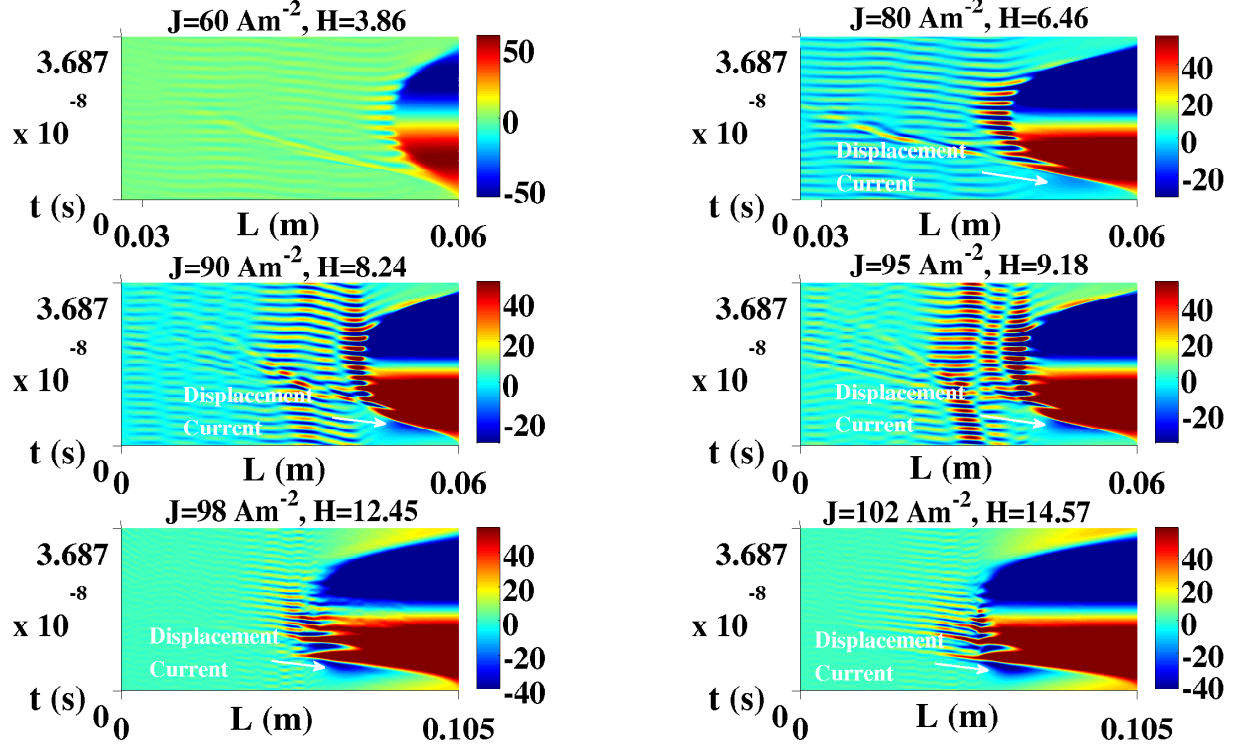


FIG. 6. Spatiotemporal profile of displacement current. Conditions : $\tilde{J}_0 = 60 - 102 \text{ A/m}^2$, $f_{rf} = 27.12 \text{ MHz}$, $H \approx 3.86 - 14.57$, $T_e = 2.5 \text{ eV}$, $T_i = 0.03 \text{ eV}$ at argon plasma density $= 3.0 \times 10^{15} \text{ m}^{-3}$.

potential and bounce back from the expanding sheath towards the bulk plasma. These bounced electrons meet the low energy electrons moving towards the sheath at some point. At this position, the electron fluid is compressed and we observe a field reversal condition.

Figure 6 shows the spatio-temporal profile of the displacement current. It is well known in CCPs that in general displacement current is significant only inside the space charge sheath region and that outside the sheath, only conduction current plays an important role. However near the place where field reversal is observed, an appreciable displacement current is clearly present. The field reversal is associated with a maximum of the electrostatic potential, and the presence of a population of electrons trapped in the corresponding potential well.

Figure 7 shows the spatio-temporal profile of charge separation *i.e.* $(n_e - n_i)$. This figure indicates trapping of electrons near to the sheath edge at the time of sheath expansion for higher values of H . This is the same region where field reversal is present. For lower values of H , there is no field reversal and no electron trapping. Electrons move from the bulk plasma

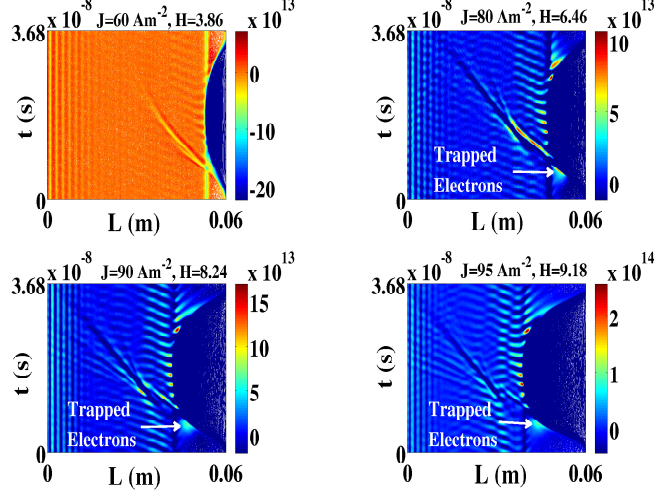


FIG. 7. Spatiotemporal profile of charge separation ($n_e - n_i$) for different values of H . Electrons are trapped near the sheath edge during the time of sheath expansion for higher values of H . Conditions : $\tilde{J}_0 = 60 - 95 \text{ A/m}^2$, $f_{rf} = 27.12 \text{ MHz}$, $H \approx 3.86 - 9.18$, $T_e = 2.5 \text{ eV}$, $T_i = 0.03 \text{ eV}$ at argon plasma density $= 3.0 \times 10^{15} \text{ m}^{-3}$.

towards the sheath and bounce back because of a very high sheath potential. However when electrons enter the field reversal region they trap there. In steady state the presence of a population of trapped electrons is observed and because of the trapping and untrapping of these trapped electrons at the field reversal position during the sheath expansion causes electron plasma wave formation near to the sheath region.

Another interesting phenomenon occurs because of trapping and untrapping of electrons is the modification of the sheath edge. During the sheath expansion, the electrons trap at the field reversal position. When these trapped electrons become untrapped, the sheath edge modifies and waves occur just near to this modified region. The 3-D spatiotemporal figure of electron density are shown for two different cases in figure 8 and figure 9. These figure show the electron density profile for one RF cycle. The sheath structure modification and wave propagation can be seen in these figures. We have observed this type of phenomena in several other cases for different densities.

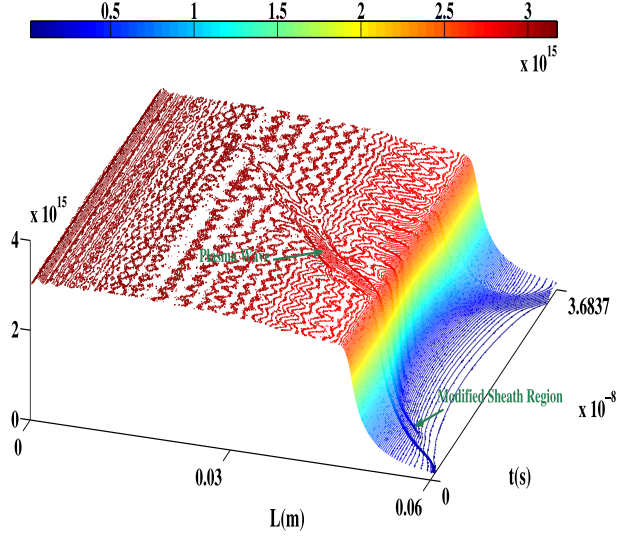


FIG. 8. A 3-D spatiotemporal profile of electron density. It shows that the sheath edge is modified and plasma waves are launched from just near to this modified region. Conditions: $\tilde{J}_0 = 80 \text{ A/m}^2$, $H = 6.46$, $T_e = 2.5 \text{ eV}$ at plasma density $= 3.0 \times 10^{15} \text{ m}^{-3}$.

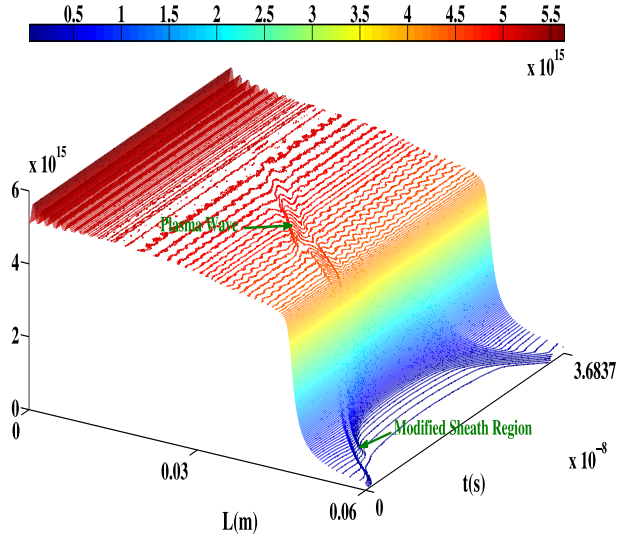


FIG. 9. A 3-D spatiotemporal profile of electron density. It shows that the sheath edge is modified and plasma waves are launched from just near to this modified region. Conditions: $\tilde{J}_0 = 120 \text{ A/m}^2$, $H = 8.974$, $T_e = 2.5 \text{ eV}$ at plasma density $= 5.0 \times 10^{15} \text{ m}^{-3}$.

A. Temporal Evolution of Wave: Evidence of Electron Plasma Wave

In this section we investigate whether these oscillations are either some traveling random oscillations or electron plasma waves. The frequency of these waves are calculated here

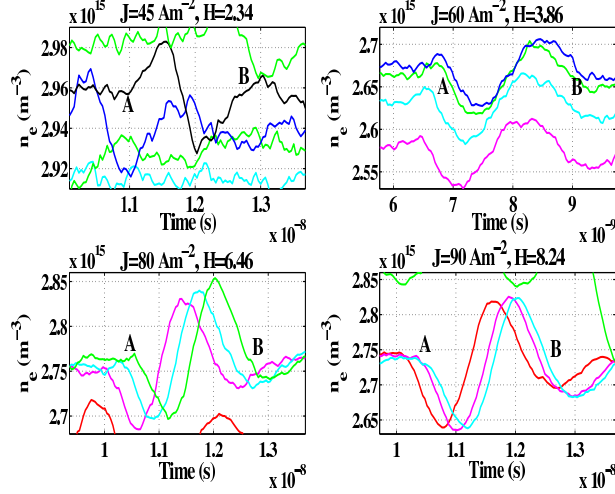


FIG. 10. This figure is zoomed part of figure 3 and shows temporal evolution of electron density n_e . Here the n_e is plotted at different positions in the system length for an RF period. For $\tilde{J}_0 = 45$ A/m² the time period of wave is calculated by plotting n_e at the position 4.28 cm (black line). Similarly for $\tilde{J}_0 = 60 - 90$ A/m² the time period of wave is calculated by plotting n_e at the position 5.24 cm (sky blue line), 4.28 cm (green line) and 3.89 cm (sky blue line) respectively. Conditions : $\tilde{J}_0 = 45 - 90$ A/m², $f_{rf} = 27.12$ MHz, $H \approx 2.34 - 8.24$, $T_e = 2.5$ eV, $T_i = 0.03$ eV at argon plasma density = 3.0×10^{15} m⁻³.

by investigation of temporal evolution of electron density which clearly indicates the wave propagation. The wave frequency can be calculated with help of time period between the points “A” and “B”, as shown in figure 10. The wave frequencies and the electron plasma frequencies in different cases are : (i) for $\tilde{J}_0 = 45$ A/m² : $\omega_{wave} = 3.56$ GHz and $(\omega_{pe})_{sim} = 3.06$ GHz. (ii) for $\tilde{J}_0 = 60$ A/m² : $\omega_{wave} = 2.81$ GHz and $(\omega_{pe})_{sim} = 2.96$ GHz. (iii) for $\tilde{J}_0 = 80$ A/m² : $\omega_{wave} = 3.11$ GHz and $(\omega_{pe})_{sim} = 2.98$ GHz. (iv) for $\tilde{J}_0 = 90$ A/m² : $\omega_{wave} = 3.17$ GHz and $(\omega_{pe})_{sim} = 2.98$ GHz. Here it is clear that wave frequency ω_{wave} is always either greater than or equal to $(\omega_{pe})_{sim}$ i.e. $\omega_{wave} \geq (\omega_{pe})_{sim}$. This is true for other cases also.

Figure 11 shows the temporal evolution of electron density, n_e . The simulation conditions are: *RF* current drive amplitude \tilde{J}_0 is 120 A/m² applied at density $n_0 = 5 \times 10^{15}$ m⁻³. The applied frequency f_{rf} is 27.12 MHz and the system length l is 0.06 m. Figure 11 shows the results for a single *RF* cycle. It is clear from this figure that a wave starts near $time \sim 9.36 \times 10^{-9}$ s and propagates with time, finally disappearing at $time \sim 2.16 \times 10^{-8}$ s.

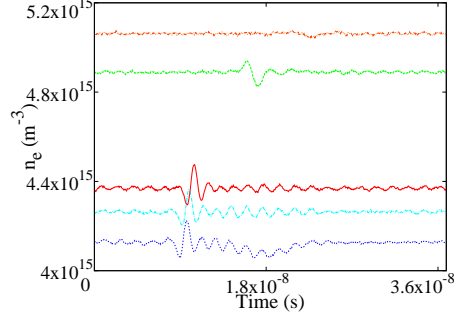


FIG. 11. Figure shows temporal evolution of electron density n_e . Conditions: $\tilde{J}_0 = 120$ A/m², $T_e = 2.5$ eV, $f_{rf} = 27.12$ MHz at plasma density = 5×10^{15} m⁻³.

FIG. 12. Figure shows zoomed in figure shows temporal evolution of electron density n_e . Conditions: $\tilde{J}_0 = 120$ A/m², $T_e = 2.5$ eV, $f_{rf} = 27.12$ MHz at plasma density = 5×10^{15} m⁻³.

The frequency of these waves can be calculated by figure 12 which is zoomed part of figure 11. The frequency can be calculated by calculating the time period between “A” and “B”, and it is $\omega_{wave} \approx 3.561 \times 10^9$ Hz. The electron plasma frequency $(\omega_{pe})_{sim}$ is 3.568×10^9 Hz here. So $\omega_{wave} \approx (\omega_{pe})_{sim}$ and it shows the signature of electron plasma waves.

B. Dependence of wave amplitude on current density amplitude

The study of dependence of the wave amplitude on the current density amplitude, \tilde{J}_0 or H is very interesting topic and is investigated here. In the literature^{11,23,38}, it is reported that the wave amplitude is enhanced as the ratio of the drift velocity to the thermal velocity

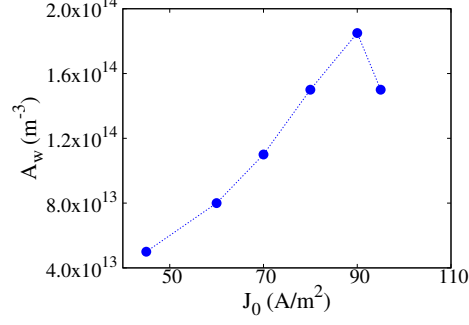


FIG. 13. Figure shows variation of wave amplitude with current density amplitude \tilde{J}_0 . Conditions : $T_e = 2.5$ eV, $f_{rf} = 27.12$ MHz and plasma density is $3 \times 10^{15} \text{ m}^{-3}$

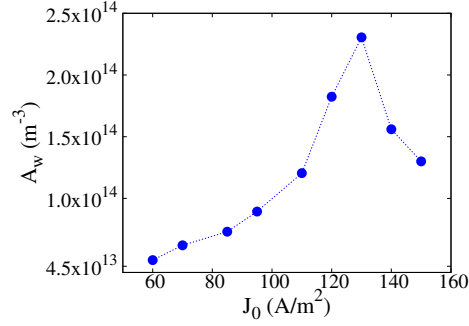


FIG. 14. Figure shows variation of wave amplitude with current density amplitude \tilde{J}_0 . Conditions : $T_e = 2.5$ eV, $f_{rf} = 27.12$ MHz and plasma density is $5 \times 10^{15} \text{ m}^{-3}$.

increases. Hence increasing \tilde{J}_0 means increasing drift velocity. The thermal velocity is nearly constant here.

Figure 13 and figure 14 shows the plot of wave amplitude (A_w) versus \tilde{J}_0 for the two different densities *i.e.* $3 \times 10^{15} \text{ m}^{-3}$ and $5 \times 10^{15} \text{ m}^{-3}$ respectively. Figure 13 shows that the wave amplitude first increases from $\tilde{J}_0 \sim 45 \text{ A/m}^2$ to $\tilde{J}_0 \sim 90 \text{ A/m}^2$. If we increase \tilde{J}_0 further, the wave amplitude drops at $\tilde{J}_0 \sim 95 \text{ A/m}^2$. The wave disappear at $\tilde{J}_0 > 95 \text{ A/m}^2$ and a new regime appear. In this new regime, the density of the bulk plasma suddenly increases because of the ion reflection which occur due to the presence of strong field reversal near sheath region at the time of sheath expansion. Figure 15 shows the trajectory of ions in velocity phase space for the case of $\tilde{J}_0 = 98 \text{ A/m}^2$. Here the positive velocity indicates direction towards the sheath (or electrode) and a negative velocity indicates direction towards the bulk plasma *i.e.* opposite to the sheath. In simulation, the trajectory of a few thousand ions are saved, out of which few ion trajectories show that ions are reflected back to the bulk plasma from

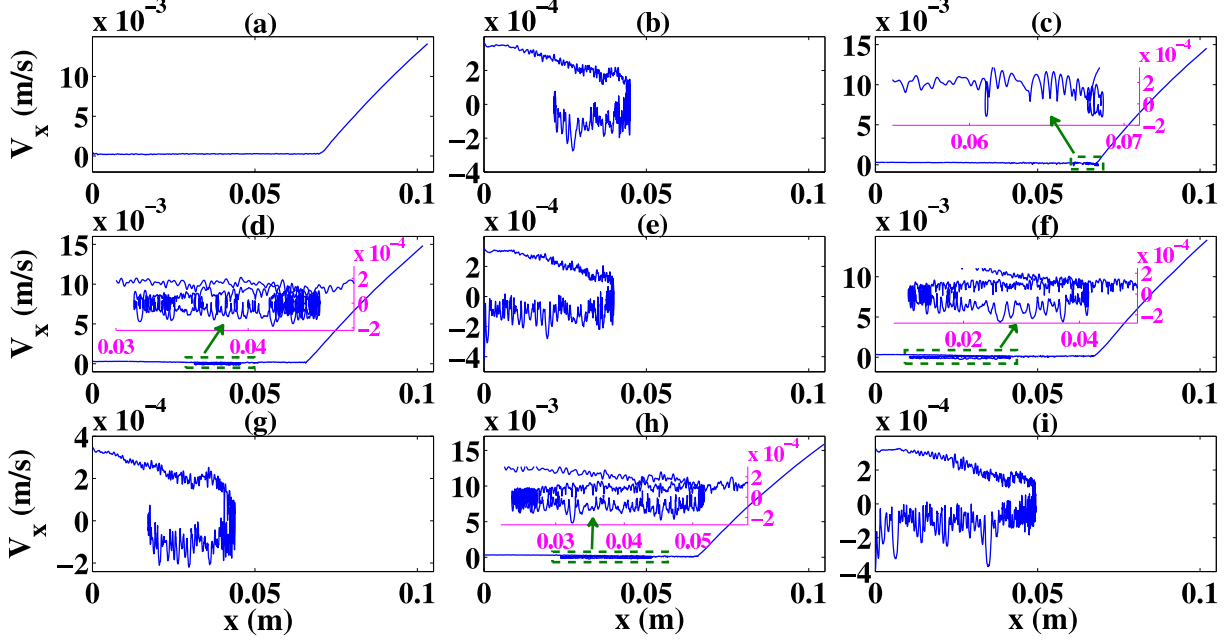


FIG. 15. Figure shows the trajectories of ions in velocity phase space. Here case (a) shows that ion propagate towards the sheath without any deflection in bulk plasma, enter inside the sheath and finally hit the electrode. The majority of ions in simulation shows this type of behavior. All other cases show the reflection of ions from near the sheath region. Conditions : $\tilde{J}_0 = 98 \text{ A/m}^2$, $T_e = 2.5 \text{ eV}$, $f_{rf} = 27.12 \text{ MHz}$ and plasma density is $3 \times 10^{15} \text{ m}^{-3}$.

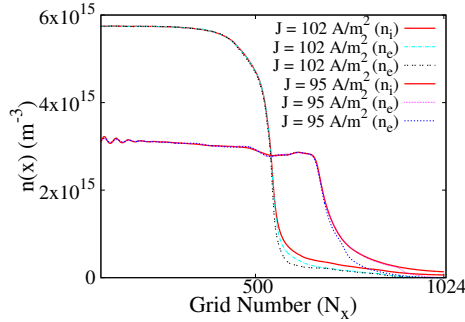


FIG. 16. Averaged ion and snapshots of electron density profile for $\tilde{J}_0 = 95 \text{ A/m}^2$ and $\tilde{J}_0 = 102 \text{ A/m}^2$ at plasma density $3 \times 10^{15} \text{ m}^{-3}$. Conditions: $T_e = 2.5 \text{ eV}$, $T_i = 0.03 \text{ eV}$, $f_{rf} = 27.12 \text{ MHz}$.

near the sheath edge. Figure 16 shows the average ion and snapshots of electron density profile for $\tilde{J}_0 = 95 \text{ A/m}^2$ and $\tilde{J}_0 = 102 \text{ A/m}^2$ at density $3 \times 10^{15} \text{ m}^{-3}$. It is clear from this figure that the density jumps from $3 \times 10^{15} \text{ m}^{-3}$ to $5.7 \times 10^{15} \text{ m}^{-3}$ when \tilde{J}_0 varies from 95 A/m^2 to 102 A/m^2 . The detailed description about ion reflection phenomena is given in

literature^{41,42}.

Similarly, figure 14 shows that the wave amplitude first increases from $\tilde{J}_0 \sim 60$ A/m² to $\tilde{J}_0 \sim 130$ A/m². If we increase \tilde{J}_0 further, the wave amplitude drops at $\tilde{J}_0 \sim 140 - 150$ A/m². So both results indicate that initially the wave amplitude increases as the ratio of drift velocity to thermal velocity increases, confirming the argument reported in the literature. On the other hand, the present results show that—at constant plasma density—the wave amplitude is a maximum at a particular \tilde{J}_0 (*i.e.* 90 A/m² for $n_0 = 3 \times 10^{15}$ m⁻³ and 130 A/m² for $n_0 = 5 \times 10^{15}$ m⁻³). Beyond this point, the wave amplitude decreases rapidly, although the ratio of drift velocity to the thermal velocity increases.

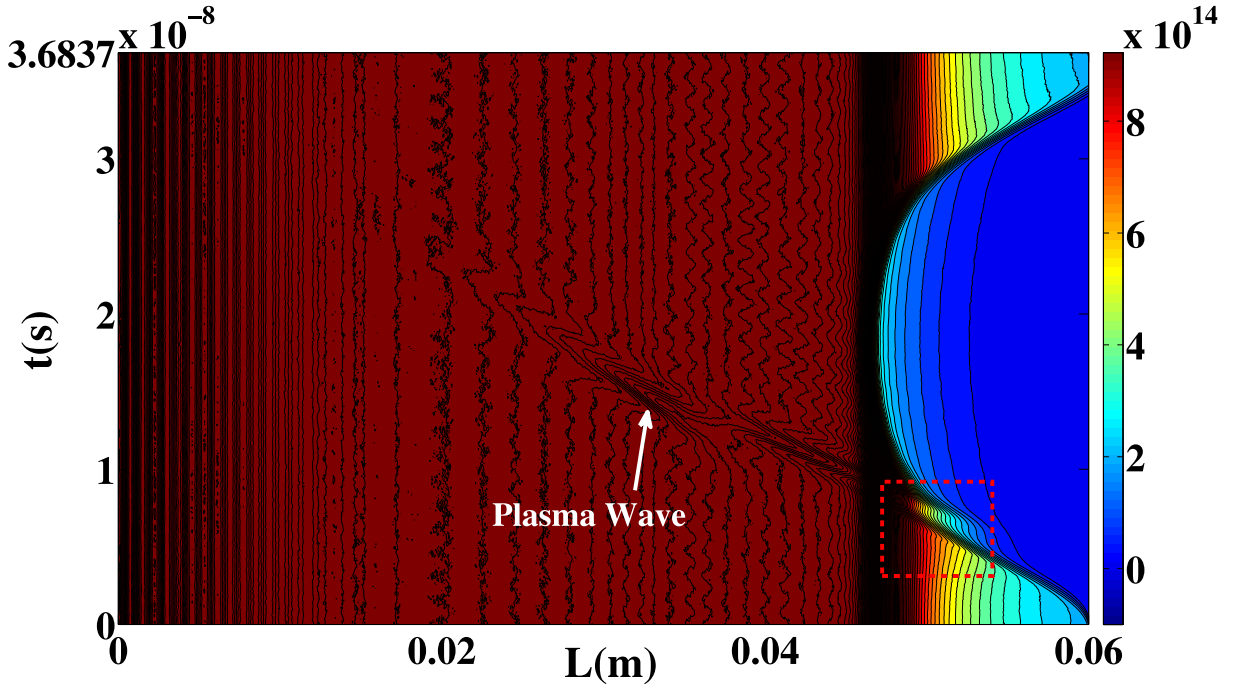


FIG. 17. Spatiotemporal profile of electron density (n_e) for collisionless case. The modified sheath region is enclosed by rectangle box shown in figure. Conditions : $\tilde{J}_0 = 120$ A/m², $T_e = 2.5$ eV, $f_{rf} = 27.12$ MHz and plasma density is 5×10^{15} m⁻³.

IV. EFFECT OF COLLISIONS ON WAVES

In practice, the charged particles have a finite mean free path, contrary to the assumption of the preceding sections. In this section, we will investigate the effect of electron elastic collisions on the electron plasma waves. Simulation results show that in the collisionless case,

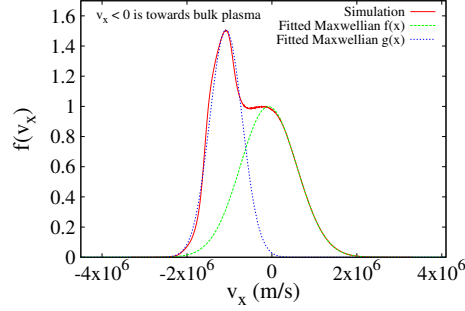


FIG. 18. Figure shows the electron velocity distribution function in modified sheath region (area enclosed by rectangle box) in figure 17. Electrons propagate towards bulk plasma for $v_x < 0$.

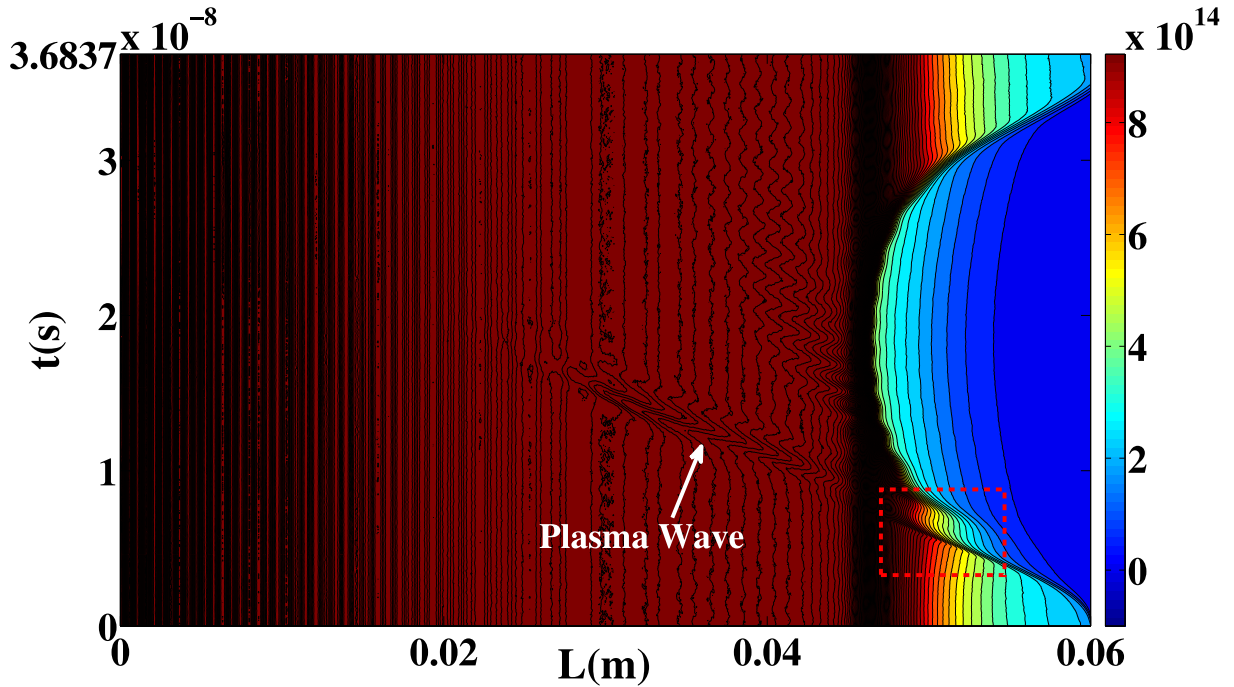


FIG. 19. Spatiotemporal profile of electron density (n_e) at pressure 20 mTorr. The modified sheath region is enclosed by a rectangle box as shown. Conditions : $\tilde{J}_0 = 120$ A/m², $T_e = 2.5$ eV, $f_{rf} = 27.12$ MHz and plasma density is 5×10^{15} m⁻³.

electron plasma waves occur near the sheath edge and propagate towards the bulk plasma. The amplitude of these waves damp and finally the waves disappear. This happens because of the Landau damping phenomena. Here the results of collisionless case are compared with the results at different pressures *i.e.* 20 mTorr and 100 mTorr. All simulation runs are for argon discharges. The usual Monte Carlo procedure is used to model these collisional interactions. Input parameters are, $J_{rf} = 120$ A/m², $f_{rf} = 27.12$ MHz, $T_e = 2.5$ eV,

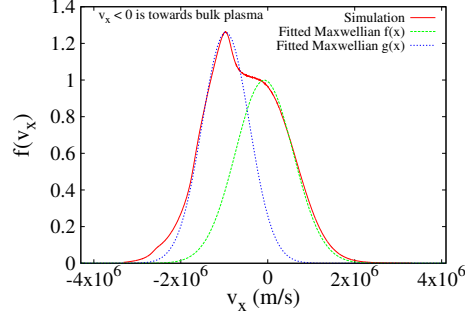


FIG. 20. Figure shows the electron velocity distribution function in the modified sheath region (area enclosed by rectangle box) in figure 19 at pressure 20 mTorr. Electrons propagate towards bulk plasma for $v_x < 0$.

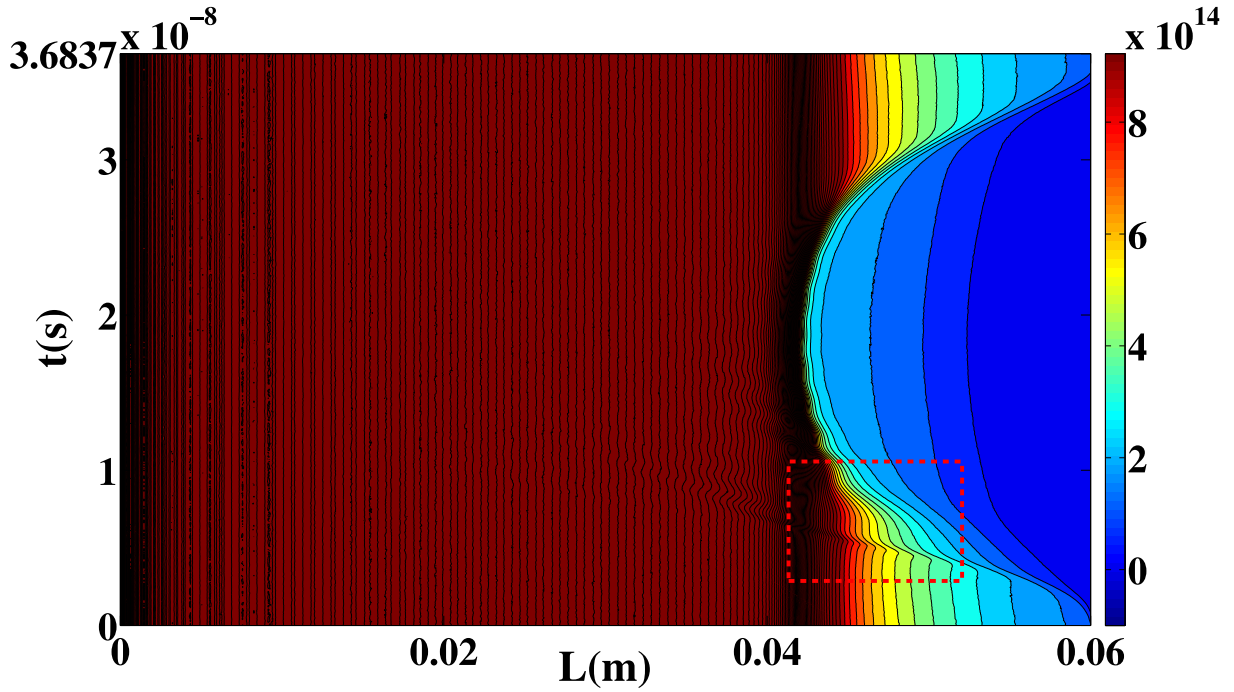


FIG. 21. Spatiotemporal profile of electron density (n_e) at pressure 100 mTorr. The modified sheath region is enclosed by a rectangle box as shown. Conditions : $\tilde{J}_0 = 120 \text{ A/m}^2$, $T_e = 2.5 \text{ eV}$, $f_{rf} = 27.12 \text{ MHz}$ and argon plasma density is $5 \times 10^{15} \text{ m}^{-3}$.

$T_i = 0.03 \text{ eV}$ and the density is $5 \times 10^{15} \text{ m}^{-3}$.

Figure 17 shows the spatiotemporal profile of electron density for the collisionless case where the modified sheath region is enclosed by a rectangular box. During the sheath expansion, the area near the sheath edge distorts significantly and the wave starts near to this region. Figure 18 represents the electron velocity distribution function in the modified

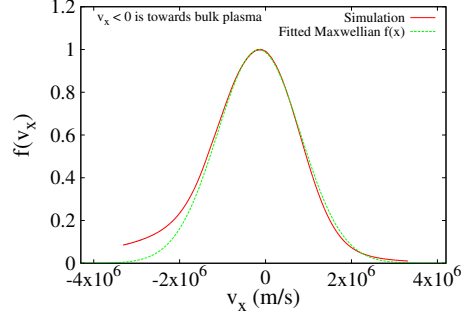


FIG. 22. Figure shows the electron velocity distribution function in the modified sheath region (area enclosed by rectangle box) in figure 21 at pressure 100 mTorr. Electrons propagate towards bulk plasma for $v_x < 0$.

sheath region (area enclosed in rectangular box). It is clear from figure 18 that the two Maxwellian curves are well fitted with the simulation results. Here $v_x < 0$ represents the electrons move towards bulk plasma (opposite to the sheath region) and $v_x > 0$ represents electrons travel towards the sheath region. Here the y-axis has arbitrary units. The fitted Maxwellian functions are given by

$$\begin{aligned} f(x) &= A \exp(B(x - x_0)^2) \\ g(x) &= A' \exp(3B(x - x'_0)^2) \end{aligned} \quad (3)$$

where A and A' represents the amplitude of the Maxwellian functions and B represents $-m_e/2k_B T_e$. However it is clear from function $g(x)$ that a beam of high velocity electrons comes out from the modified sheath region and penetrates into the bulk plasma. The electron plasma waves starts near to the sheath region and finally it damps at a distance of approx 0.025 m.

Figure 19 represents the spatiotemporal profile of the electron density at 20 mTorr. Here the modified sheath region is clearly seen in the rectangular box. Figure 20 shows the electron velocity distribution function in the modified sheath region. Two Maxwellian curves are fitted with simulation data but the curve has a peak at 1×10^6 m/s, which is not much less compared to the collisionless case. Plasma waves which starts near to the sheath edge finally damp at a distance of approx 0.032 m. At high pressures *i.e.* 100 mTorr the modified sheath region almost disappears (see figure 21) inside rectangular box. The electron velocity distribution function shown by figure 22 is almost Maxwellian and well fitted by analytical expression of Maxwellian distribution. The wave phenomenon almost disappears here.

The above results indicate that in the presence of high pressure, the modified sheath region disappears and wave effects diminish very quickly.

V. CONCLUSION AND DISCUSSION

The existence of electron plasma waves near to the plasma-sheath interface has been observed and investigated. These waves have been studied by the spatial and temporal evolution of electron density. The quasi-neutrality breaks down due to the overshoot of high velocity electrons into the bulk plasma at the time of sheath expansion, and as a result electron plasma waves occur in the sheath vicinity. The particle-in-cell simulation technique in the half-infinite plasma is used here. The possibility for the oscillating energy to be transferred to electron thermal energy by the Landau damping mechanism is discussed.

The spatiotemporal profile of electron density shows that electron plasma waves start from the sheath edge and propagate towards the bulk and finally disappear after few centimeters. It is also observed that the sheath structure is modified during the sheath expansion. The spatiotemporal profile of electric field indicates the presence of strong field reversal near the modified sheath region for higher values of H . The possible reason for the field reversal is the compression and rarefaction of electron fluid when the sheath expands and collapses. The profile of charge separation shows the evidence of electron trapping near the reverse field region. The trapping and untrapping of electrons during the expansion and collapse of the sheath causes the launching of waves from near to the sheath region. The evidence of significant displacement current in this region is also observed.

The temporal evolution of electron plasma waves is discussed. The frequency of the waves, ω_{wave} is calculated and it is either greater than or equal to ω_{pe} . It indicates that these waves are electron plasma waves.

The dependence of wave amplitude on current density amplitude, \tilde{J}_0 or H is also investigated here. The amplitude of the wave increases by increasing the current density amplitude (\tilde{J}_0) from low to a maximum and finally the wave disappears at high current when a new regime appear. In this new regime, the density of the bulk plasma suddenly increases because of the ion reflection which occur due to presence of strong field reversal near sheath region.

In conclusion, the regime we have investigated appears in extreme cases, *i.e.* at higher

values of \tilde{J}_0 or H than are usual for single radio-frequency discharge experiments. However for more exotic waveforms, such as pulses^{39,40}, comparable rates of change of current are achieved, and the phenomena discussed here are likely to occur under conditions of experimental interest. Hence the present research work has possible practical relevance.

The effect of electron elastic collisions with neutrals on plasma waves is also discussed. A Monte-Carlo scheme is used in PIC simulation to handle the collisions. The wave phenomena in collisionless case is compared with the results at the pressure of 20 mTorr and 100 mTorr. We have observed that in the presence of high pressure, the modified sheath region disappears and the wave effects diminish very quickly.

VI. ACKNOWLEDGMENTS

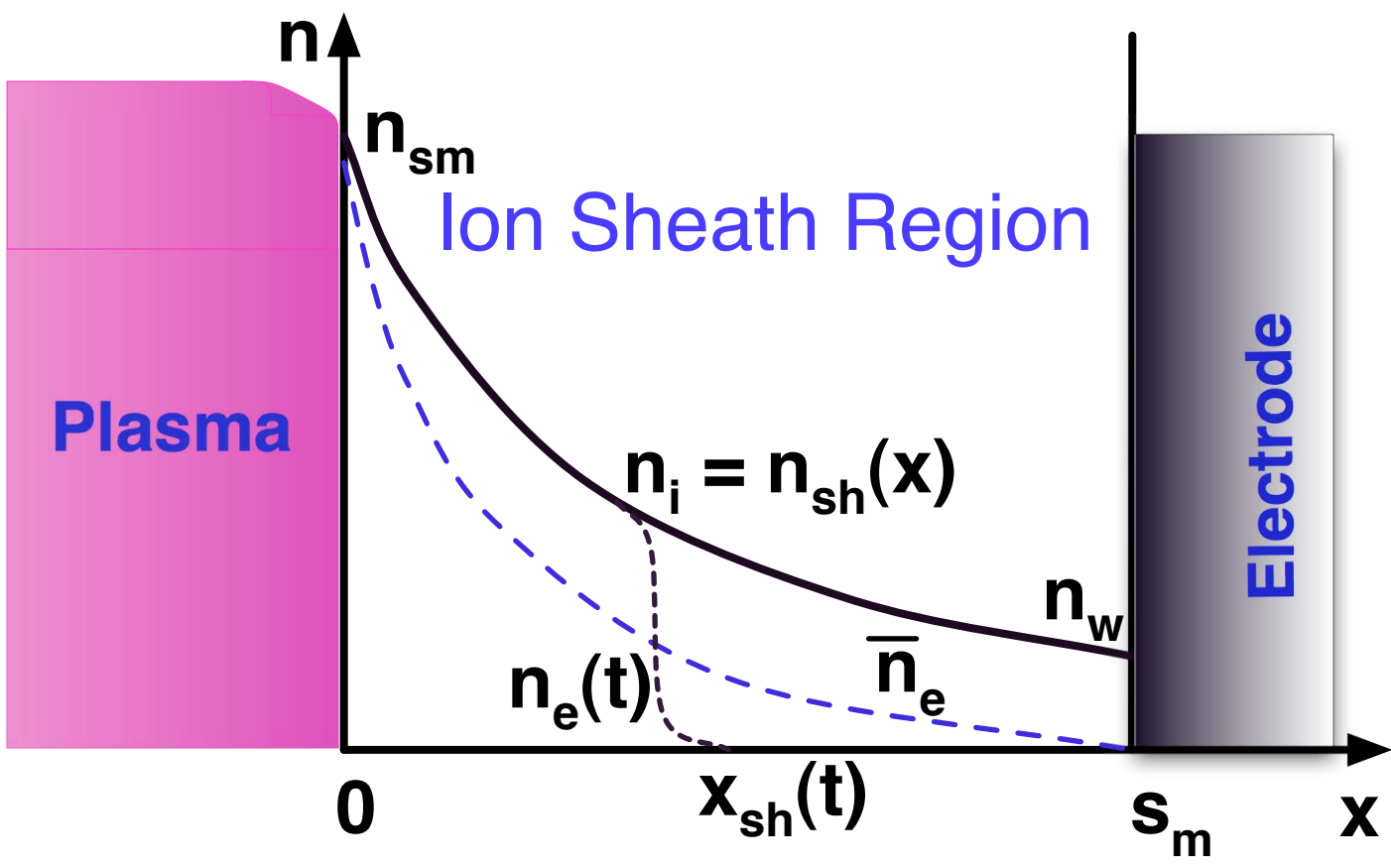
This research work is supported by Science Foundation Ireland (SFI) under grant no. 07/IN.1/1907 and 08/SRC/I1411.

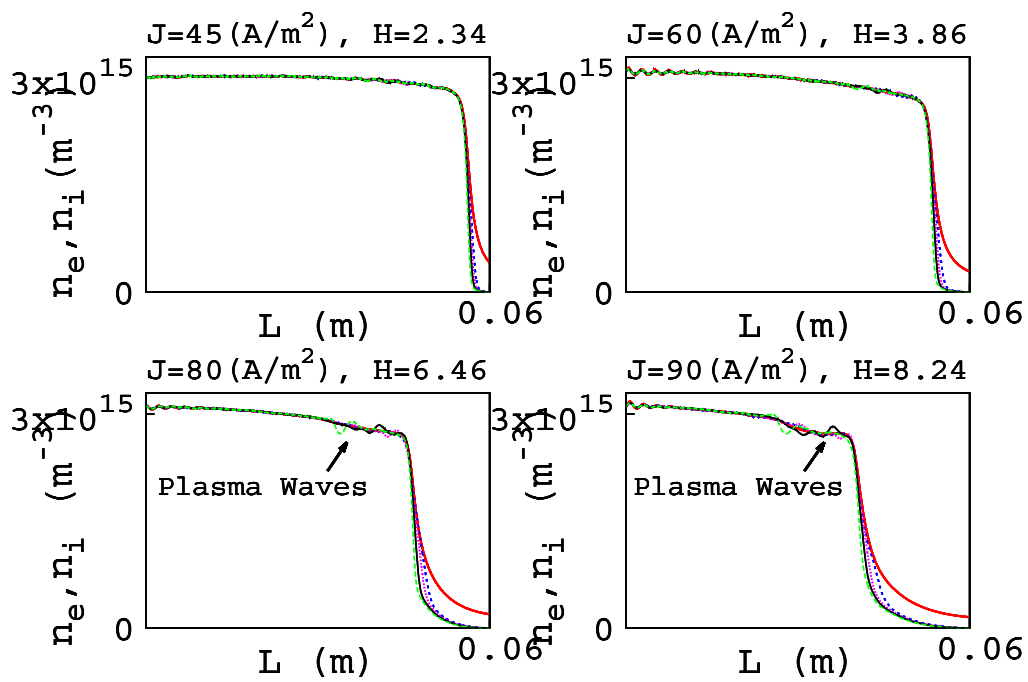
REFERENCES

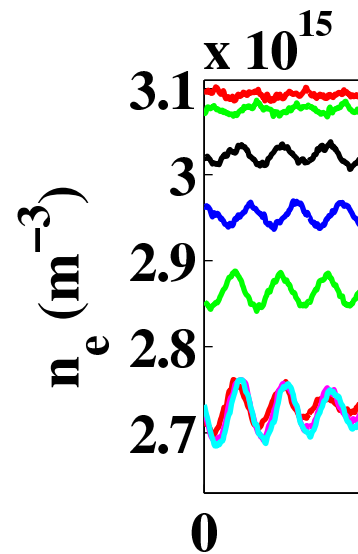
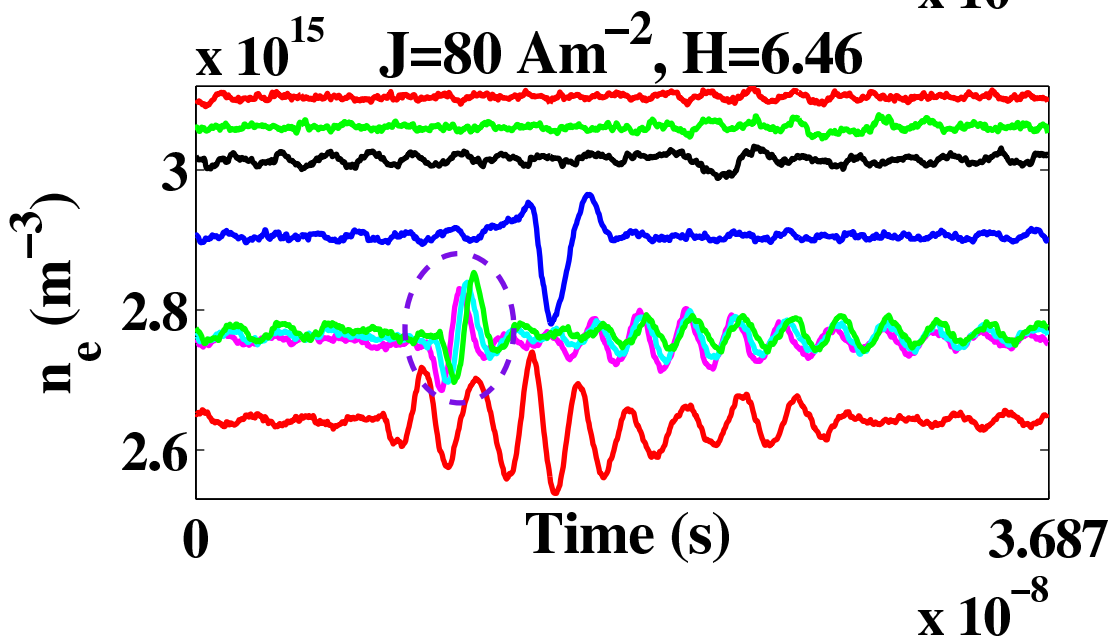
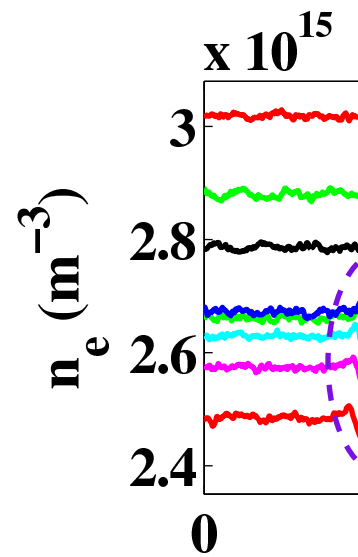
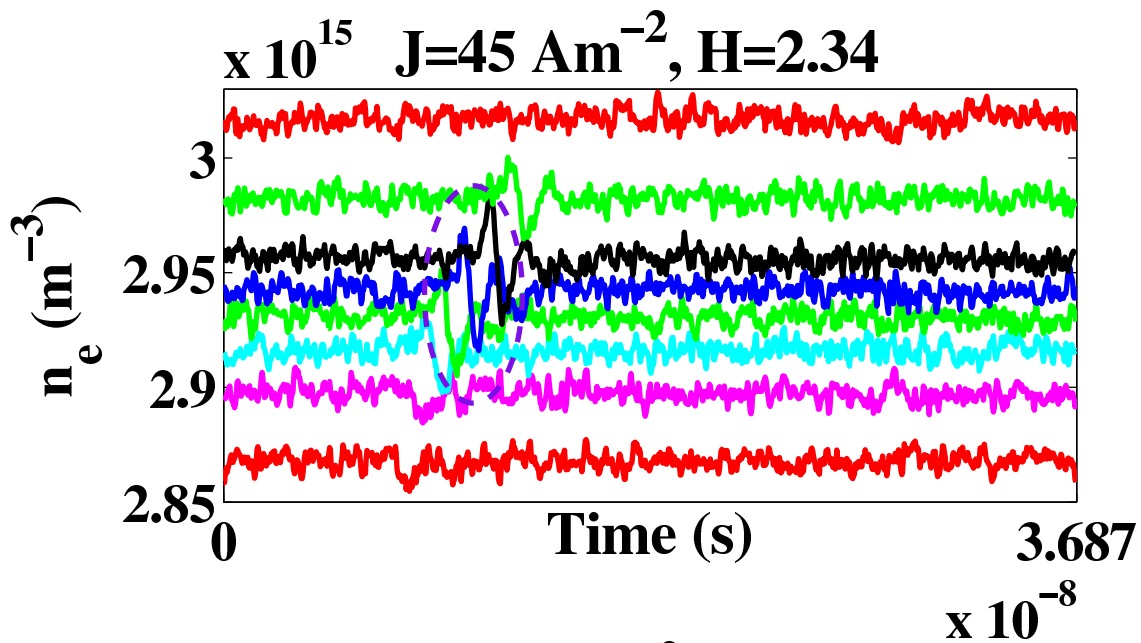
- ¹I.B. Bernstein, J.M. Greene and M.D. Kruskal, Phys. Rev. 108, 546 (1957).
- ²G. Manfredi, Phys. Rev. Lett. 79, 2815 (1997).
- ³M.V. Medvedev, P.H. Diamond, M.N. Rosenbluth and V.I. Shevchenko, Phys. Rev. Lett. 81, 5824 (1998).
- ⁴T. Gans, V.S. von der Gathen and H.F. Döbele, Europhys. Lett 66, 232 (2004).
- ⁵T. Gans, V. Schulz-von der Gathen and H.F. Döbele, Contrib. Plasma Phys. 44, 535 (2004).
- ⁶T. Gans, J. Schulze, D. O'Connell, U. Czarnetzki, R. Faulkner, A.R. Ellingboe and M.M. Turner, Appl. Phys. Lett. 89, 261502 (2006).
- ⁷D. O'Connell, T. Gans, D. Vender, U. Czarnetzki and R. Boswell, Phys. Plasmas 14, 034505 (2007).
- ⁸D. O'Connell, T. Gans, A. Meige, P. Awakowicz and R.W. Boswell, IEEE Trans. Plasma Sci. 36, 1382 (2008).
- ⁹A. Meige, D. O'Connell, T. Gans and R.W. Boswell, IEEE Trans. Plasma Sci. 36, 1384 (2008).

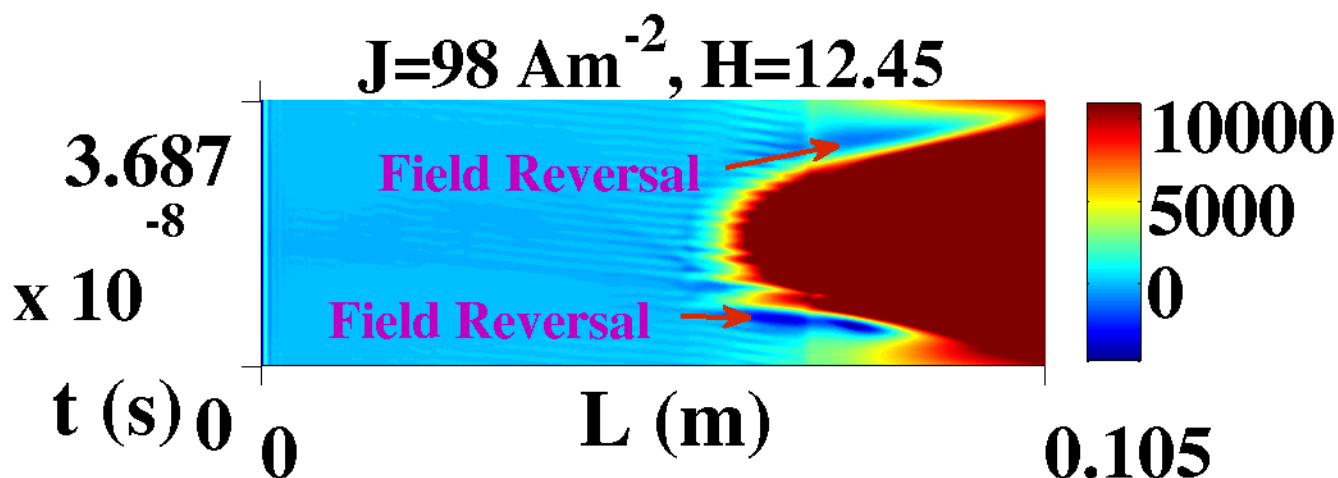
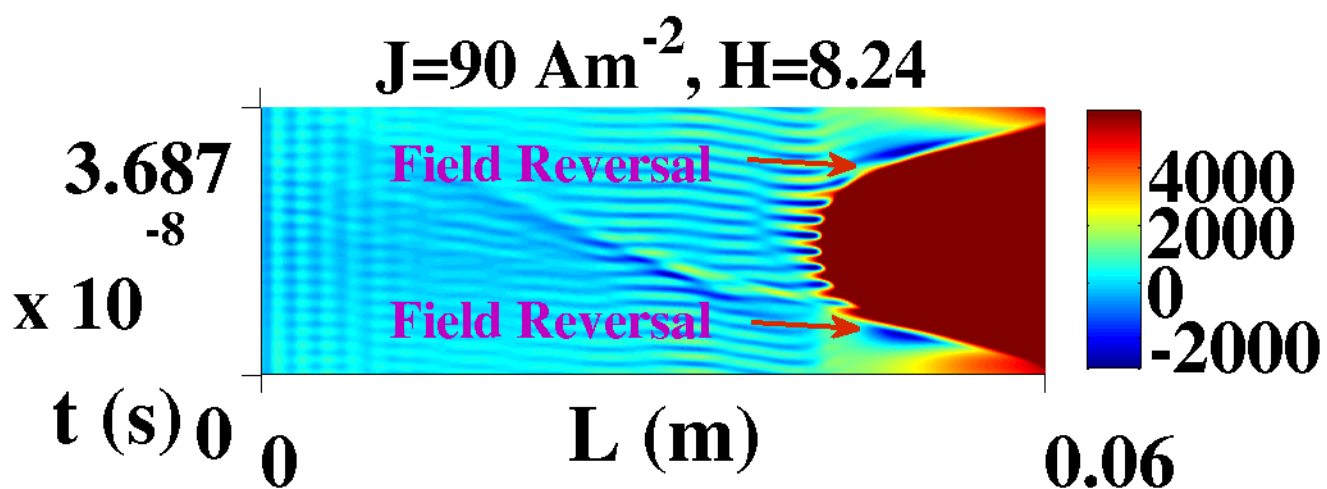
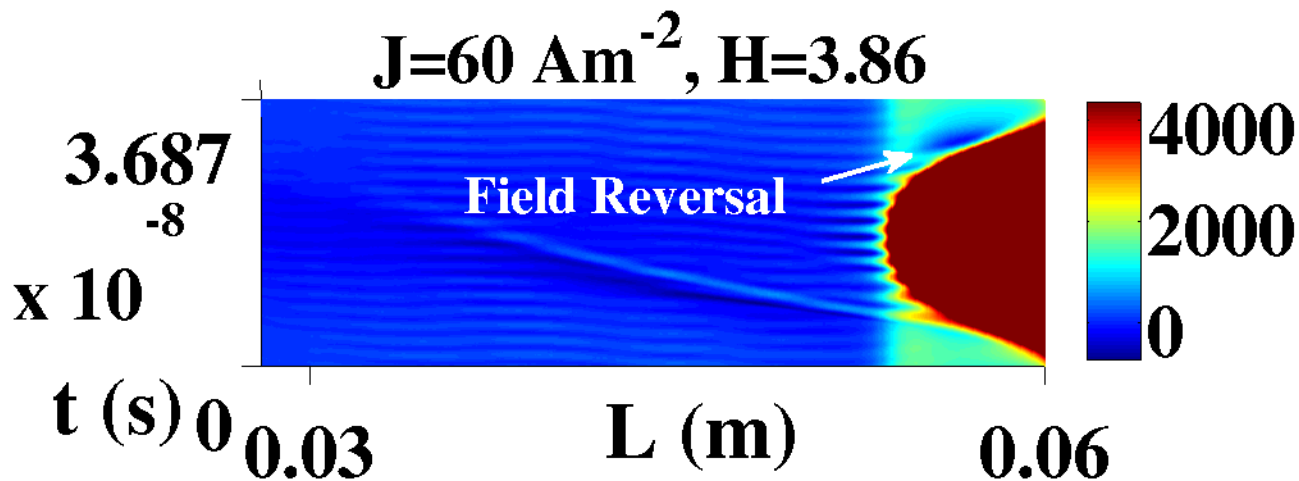
- ¹⁰G. Gozadinos, D. Vender, M.M. Turner and M.A. Lieberman, *Plasma Sources Sci. Technol.* 10, 117 (2001).
- ¹¹D. Vender and R.W. Boswell, *J. Vac. Sci. Technol. A.* 10, 1331 (1992).
- ¹²M.A. Lieberman, *IEEE Trans. Plasma Sci.* 16, 638 (1988).
- ¹³V.A. Godyak, *Sov. Phys. - Tech. Phys.* 16(7), 1073 (1972).
- ¹⁴I.D. Kaganovich, *Phys. Rev. Lett.* 89, 265006 (2002).
- ¹⁵A.I. Akhiezer and A.S. Bakai, *Sov. Phys. Dokl.* 16, 1065 (1972).
- ¹⁶M. Surendra and D.B. Graves, *IEEE Trans. Plasma Sci.* 19, 144 (1991).
- ¹⁷G. Gozadinos, M.M. Turner and D. Vender, *Phys. Rev. Lett.* 87, 135004 (2001).
- ¹⁸V.A. Godyak, *Sov. J. Plasma Phys.* 2, 78 (1976).
- ¹⁹V.A. Godyak, O.A. Popov and A.H. Khanna, *Sov. J. Plasma Phys.* 2, 560 (1976).
- ²⁰V.A. Godyak and O.A. Popov, *Sov. J. Plasma Phys.* 5, 227 (1979).
- ²¹O.A. Popov and V.A. Godyak, *J. Appl. Phys.* 57, 53 (1985).
- ²²V.A. Godyak and R.B. Piejak, *Phys. Rev. Lett.* 65, 996 (1990).
- ²³J. Borovsky, *Phys. Fluids.* 31, 1074 (1988).
- ²⁴Y.M. Aliev, I.D. Kaganovich and H. Schlüter, *Electron Kinetics and Application of Glow Discharges*, NATO ASI Series B. 367, 257 (1998).
- ²⁵Y.M. Aliev, I.D. Kaganovich and H. Schlüter, *Phys. Plasmas.* 4, 2413 (1997).
- ²⁶M. A. Lieberman and A. J. Lichtenberg, *Principles of plasma discharges and material processing*, Wiley New York (1994).
- ²⁷M.M. Turner, *Phys. Rev. Lett.* 75, 1312 (1995).
- ²⁸M. Surendra and D.B. Graves, *Phys. Rev. Lett.* 66, 1469 (1991).
- ²⁹M. Surendra and M. Dalvie, *Phys. Rev. E.* 48, 3914 (1993).
- ³⁰M.M. Turner, *Electron Kinetics and Application of Glow Discharges*, NATO ASI Series B. 367 (1998).
- ³¹L.D. Landau, *J. Phys.* 10, 25 (1946).
- ³²G. Gozadinos, D. Vender and M.M. Turner, *J. Comput. Phys.* 172, 348 (2001).
- ³³T. Gans, C.C. Lin, V. Schulz-von der Gathen and H.F. Döbele, *Phys. Rev. A, Gen. Phys.* 67, 012707 (2003).
- ³⁴M.M. Turner and M.B. Hopkins, *Phys. Rev. Lett.* 69, 3511 (1992).
- ³⁵U. Czarnetzki, D. Luggenholscher and H.F. Döbele, *Plasma Sources Sci. Technol.* 8, 230 (1999).

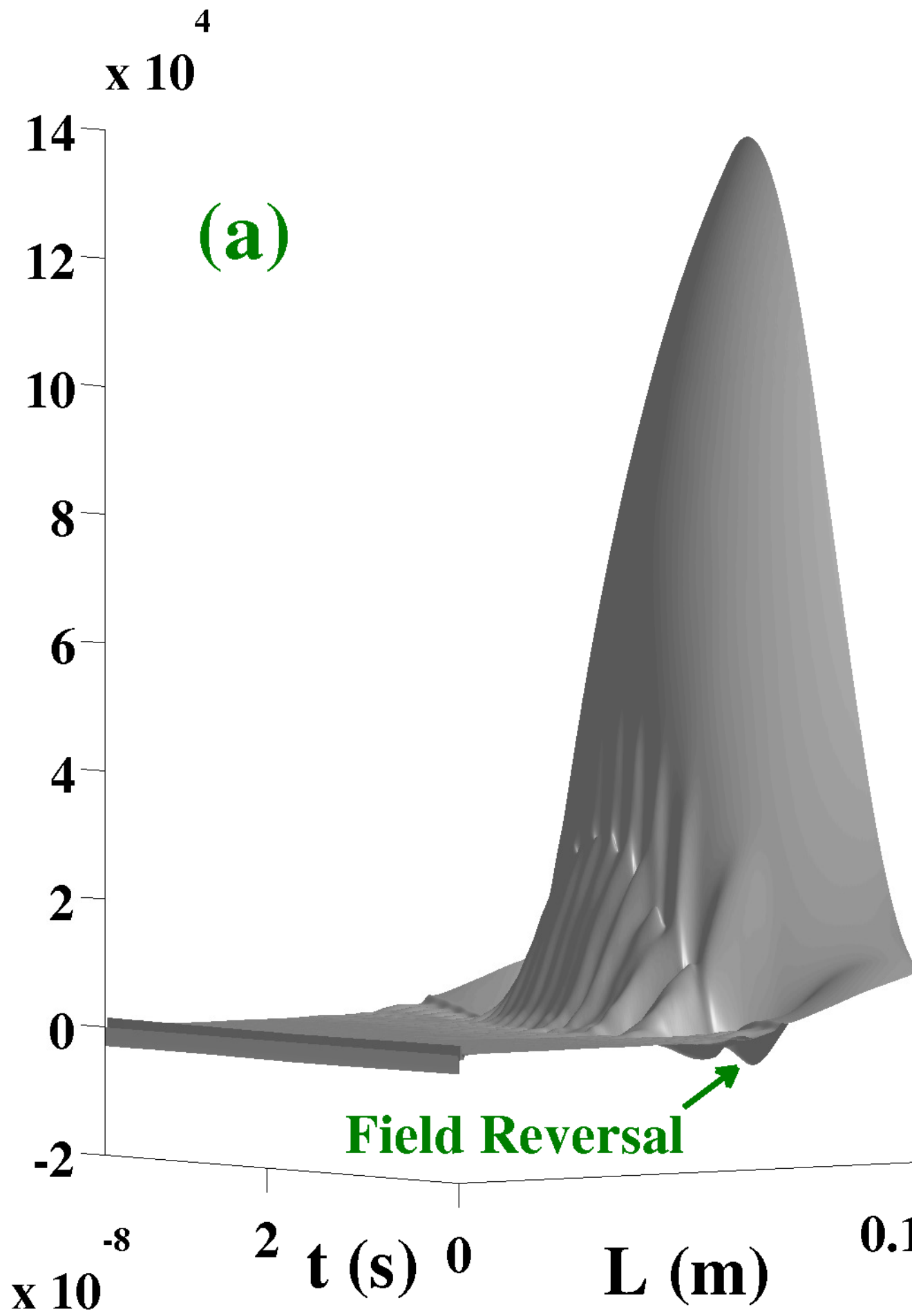
- ³⁶R.A. Gottscho, Phys. Rev. A, Gen. Phys. 36, 2233 (1987).
- ³⁷A.H. Sato and M.A. Lieberman, J. Appl. Phys. 68, 6117 (1990).
- ³⁸B.P. Wood, M.A. Lieberman and A.J. Lichtenberg, IEEE Trans. Plasma Sci. 19, 619 (1991).
- ³⁹T. Lafleur, R. W. Boswell, and J. P. Booth, Applied Phys. Lett. 100(19), 194101 (2012).
- ⁴⁰T. Lafleur, P. A. Delattre, E. V. Johnson, and J. P. Booth, Applied Phys. Lett. 101, 124101 (2012).
- ⁴¹S. Sharma and M.M. Turner, “Simulation study of stochastic heating in single frequency capacitively coupled discharges with critical evaluation of analytical models,” Plasma Sources Sci. Technol. 22(3), 035014 (2013).
- ⁴²S. Sharma , “Investigation of Ion and Electron Kinetic Phenomena in Capacitively Coupled Radio-Frequency Plasma Sheaths: A Simulation Study,” PhD Thesis, Dublin City University, Dublin, Ireland (2013).

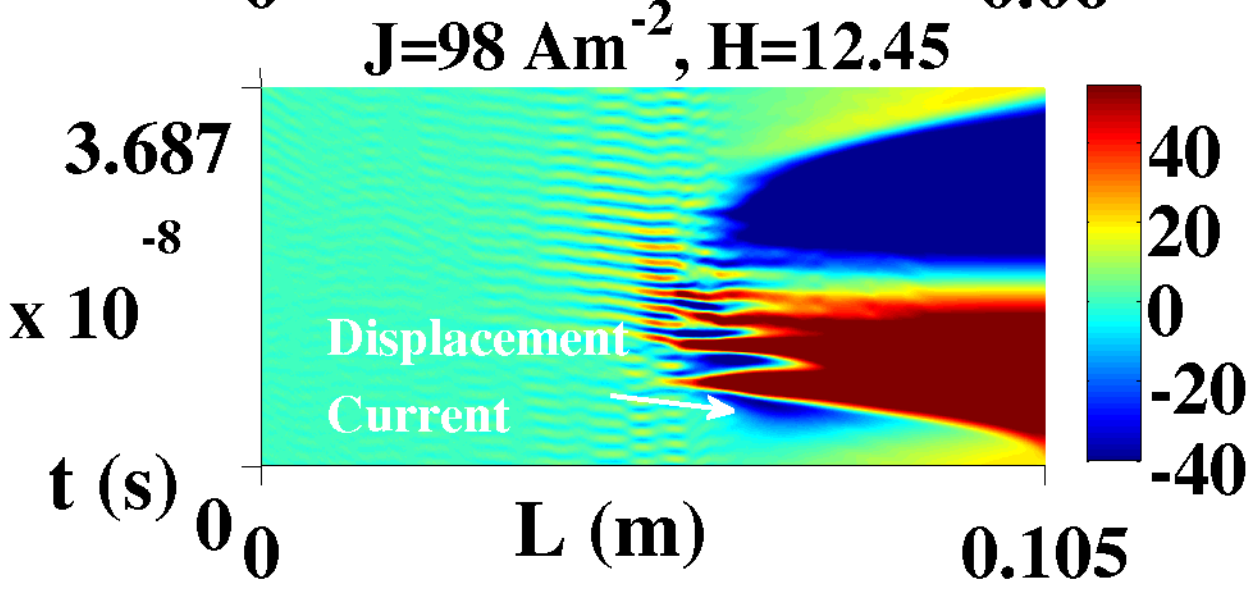
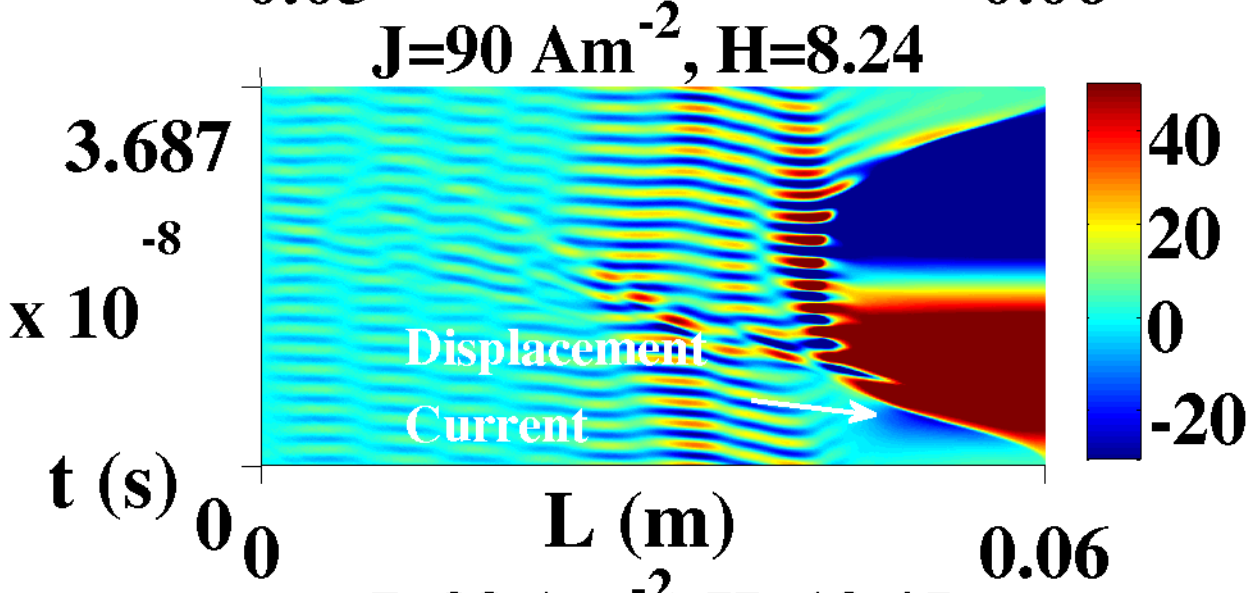
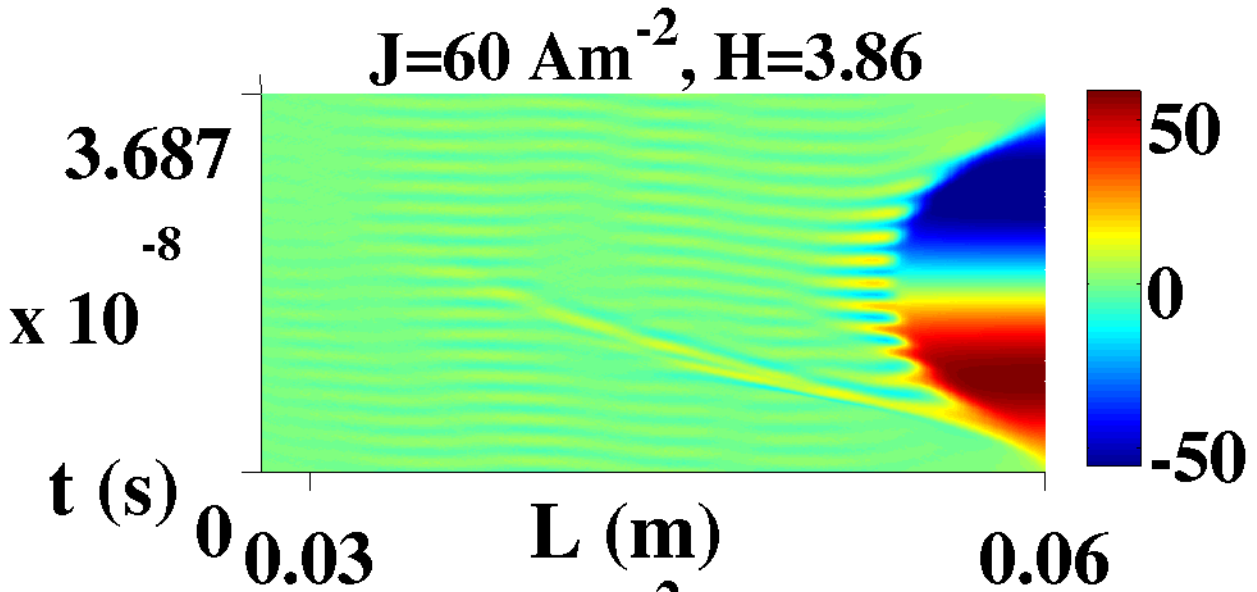


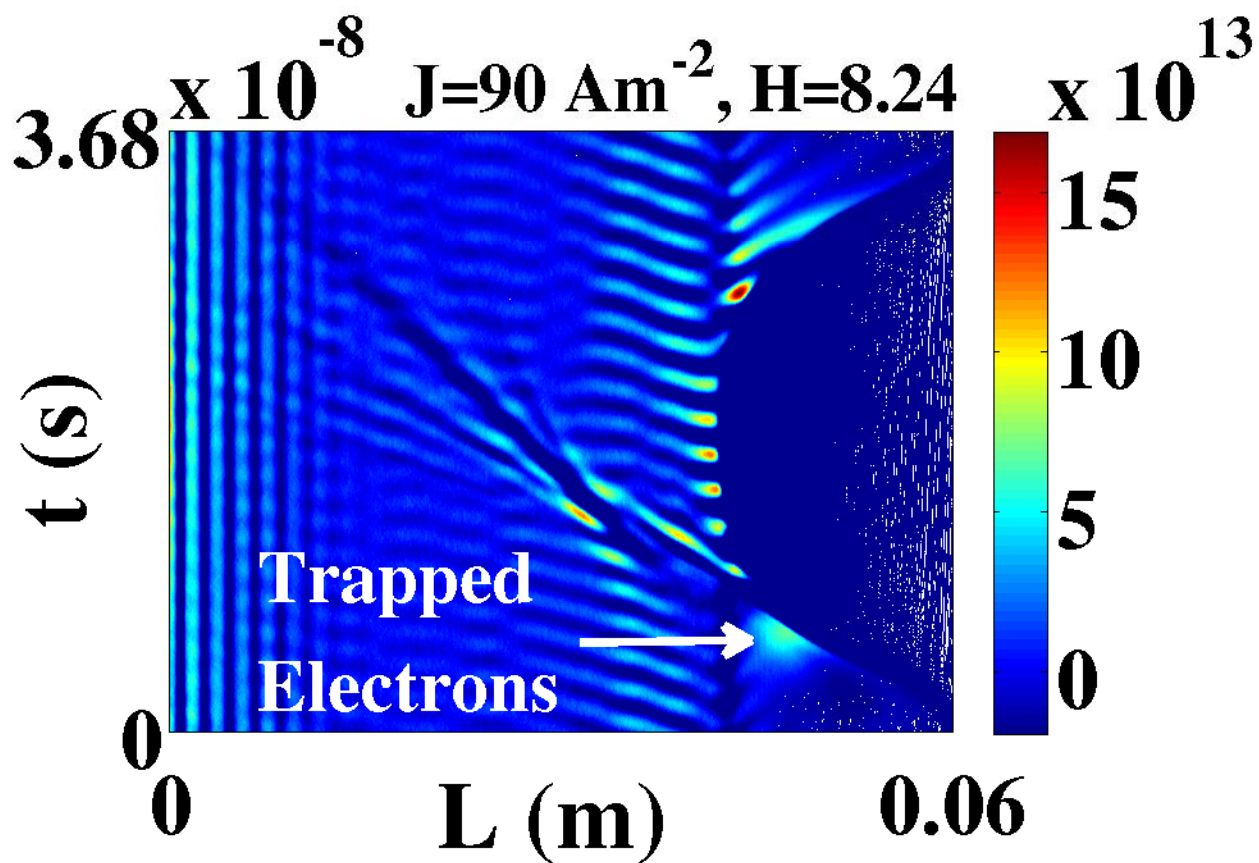
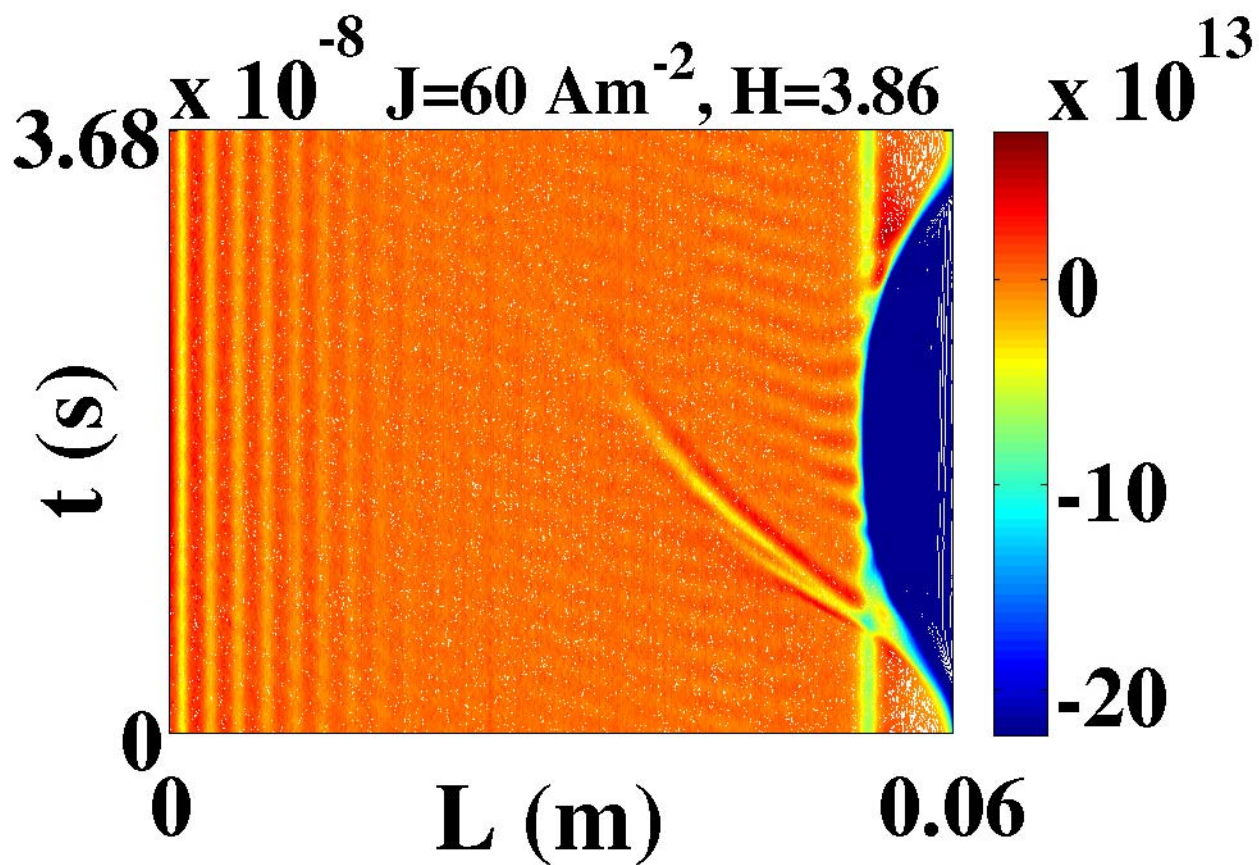






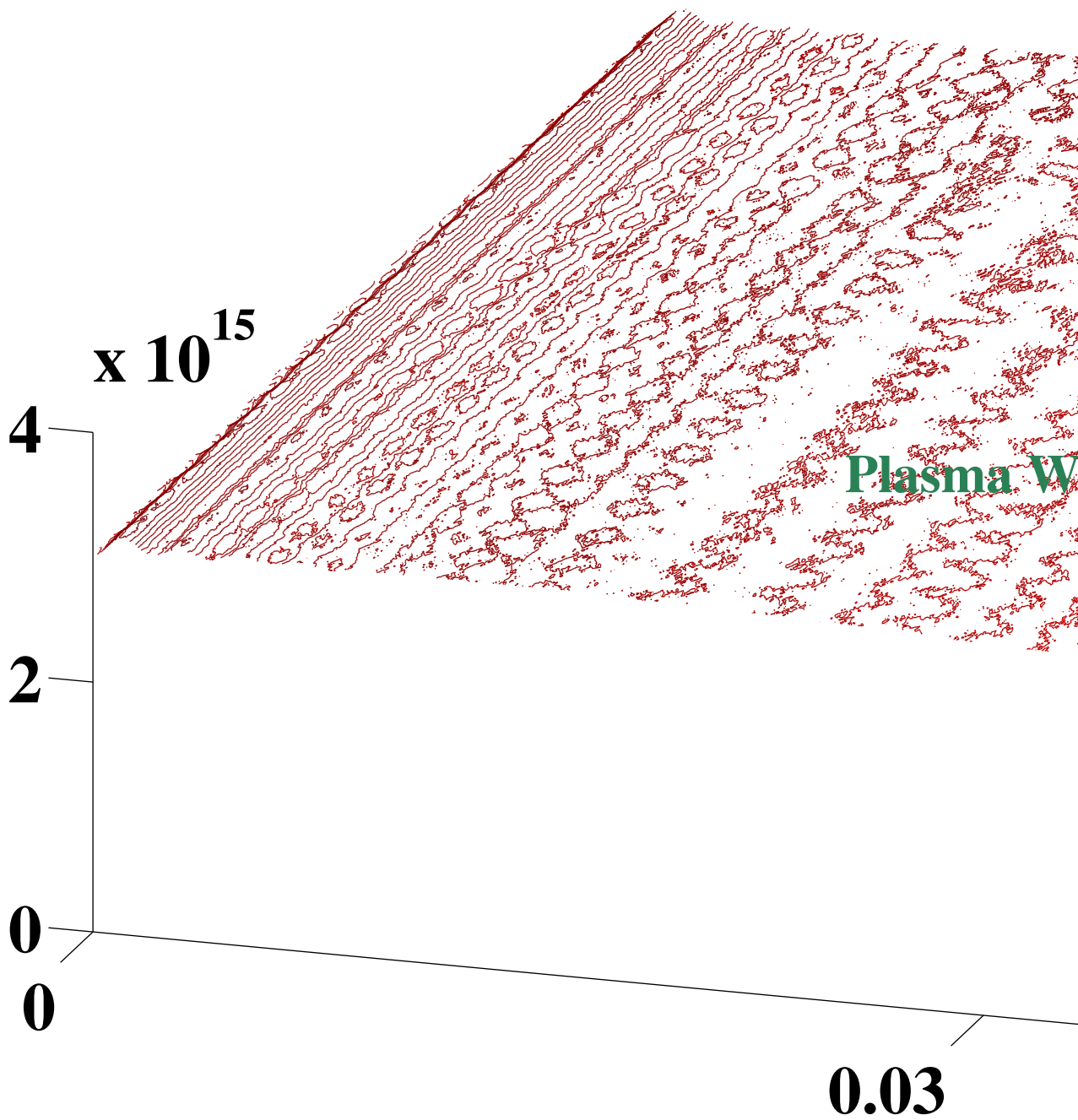


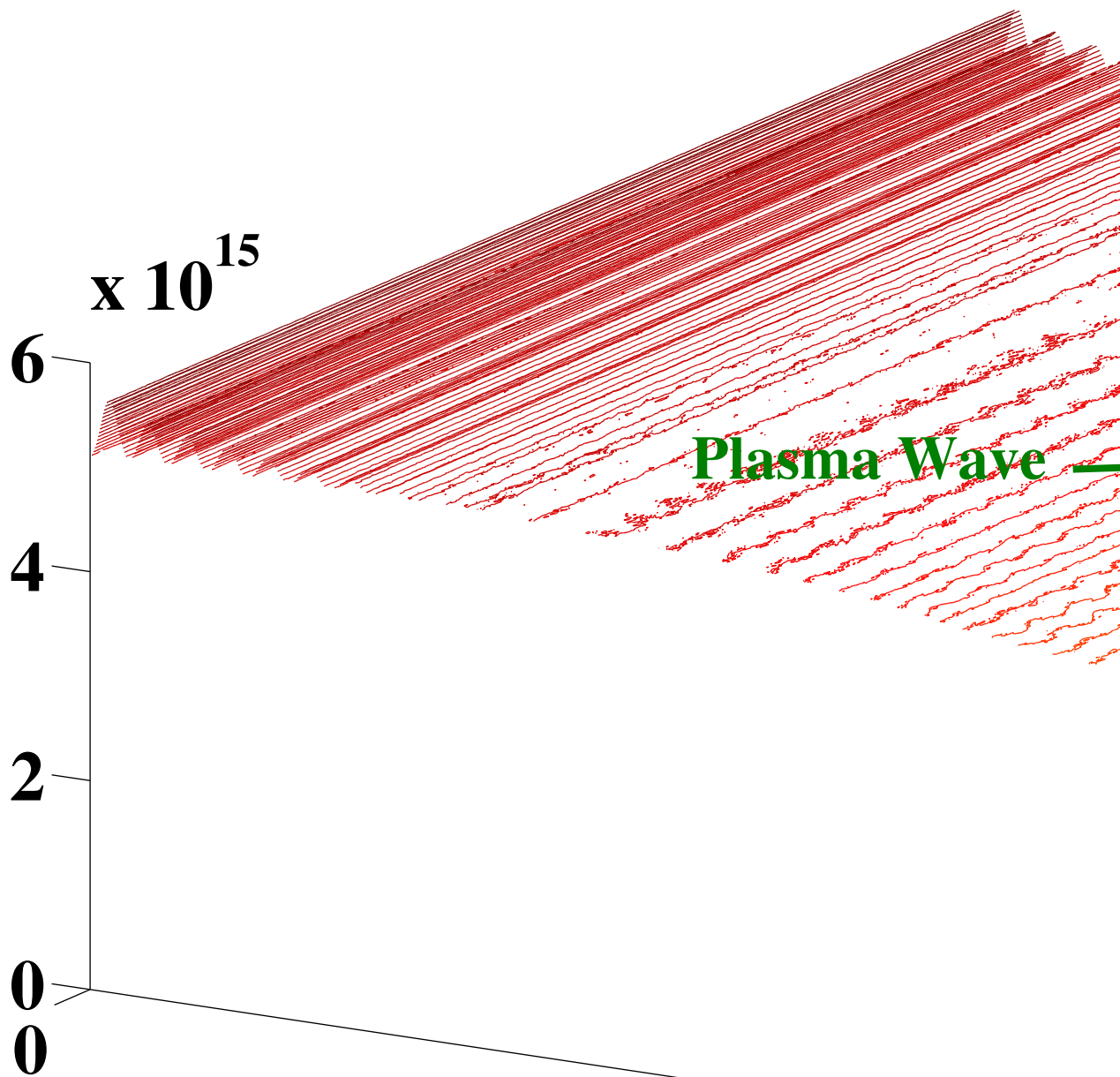
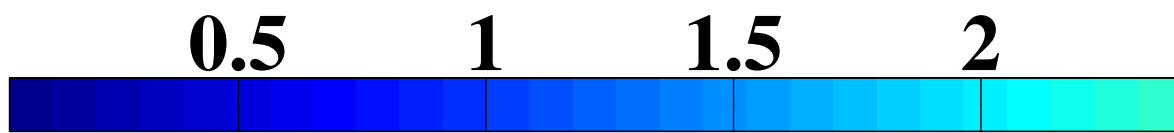




0.5

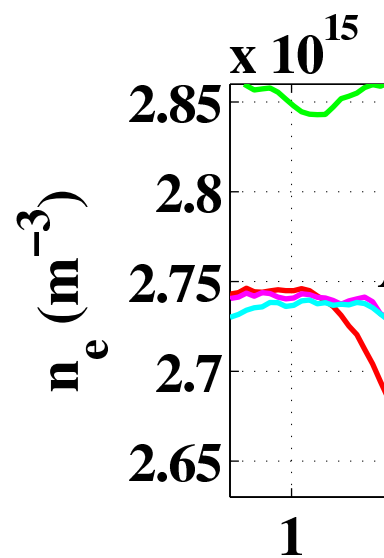
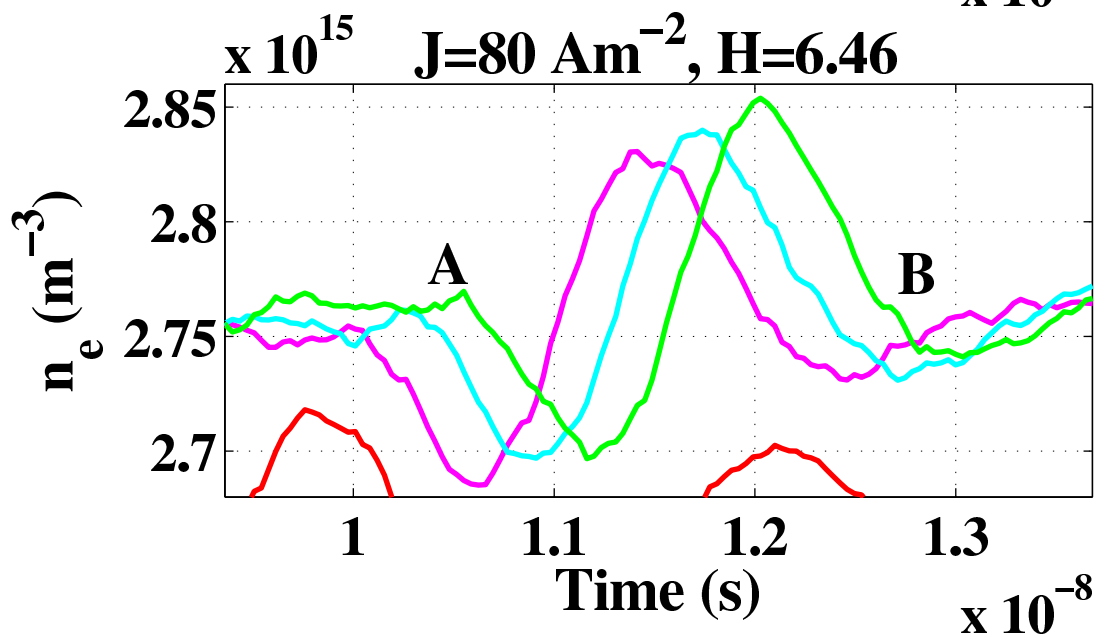
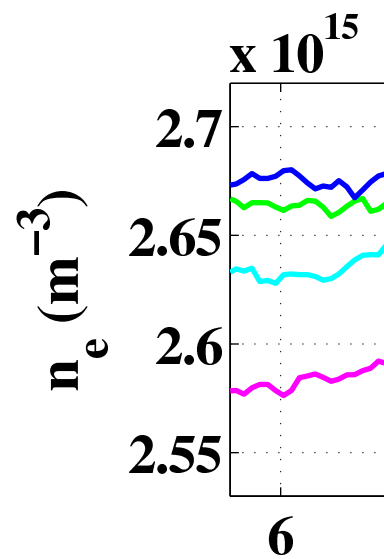
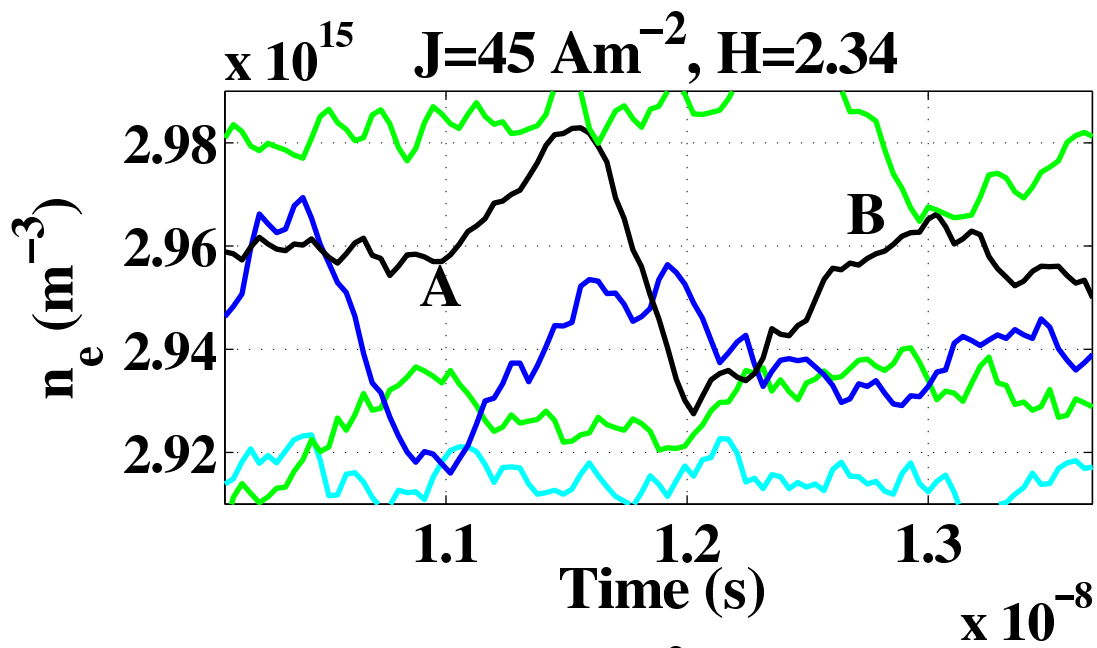
1

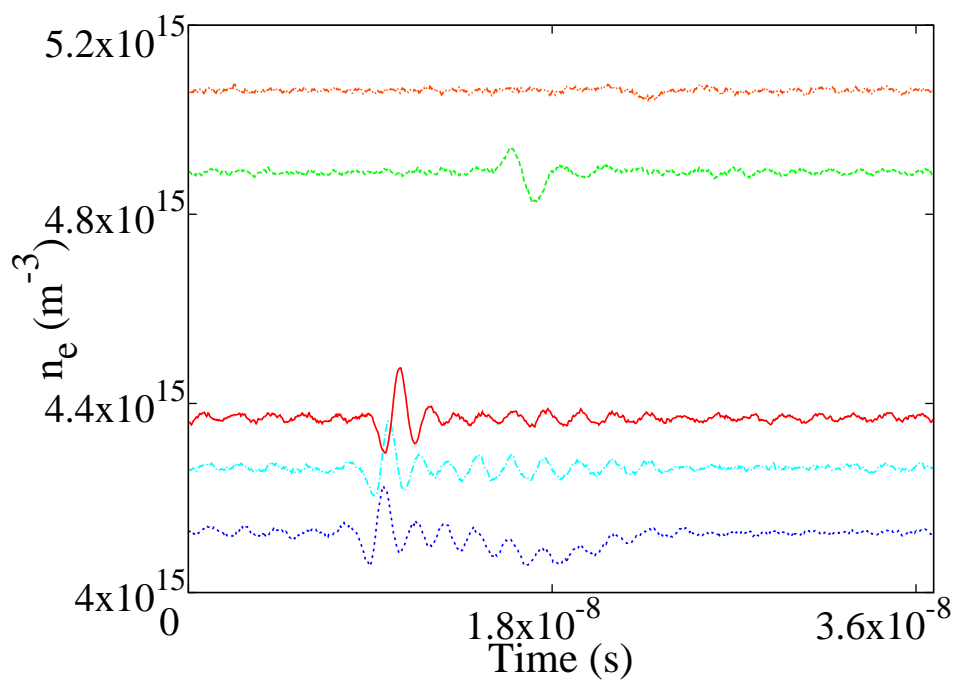


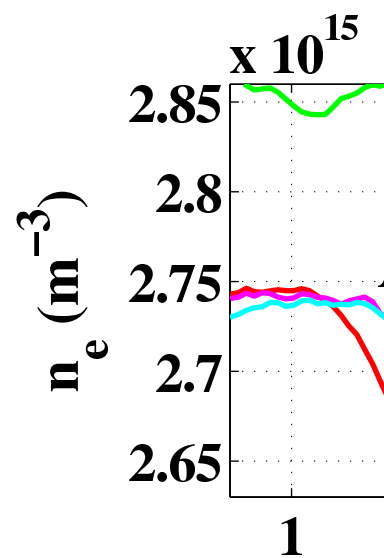
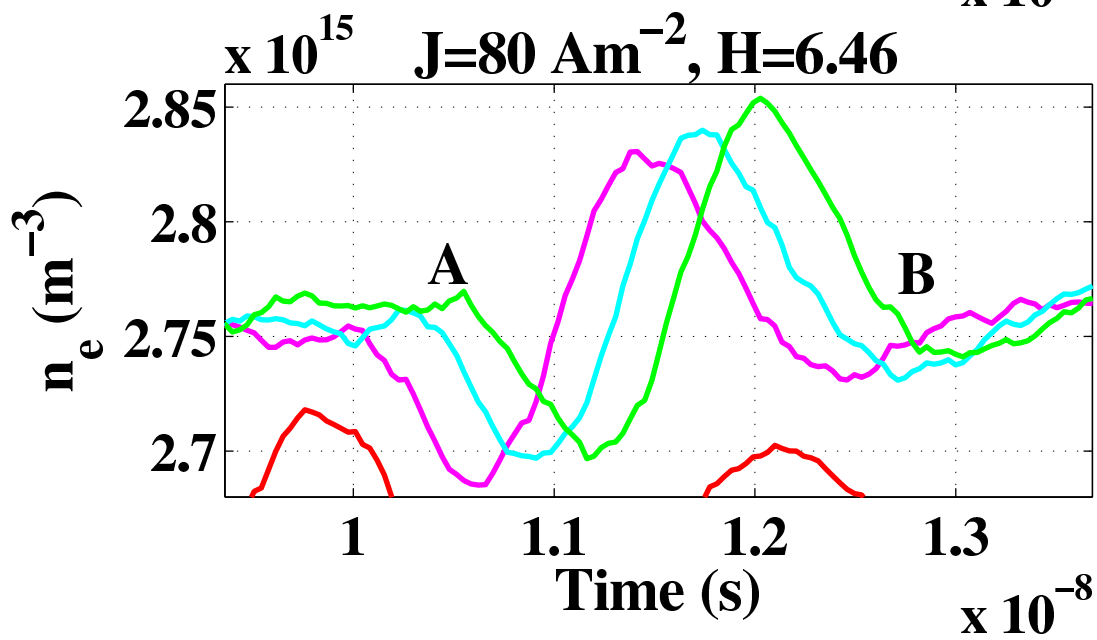
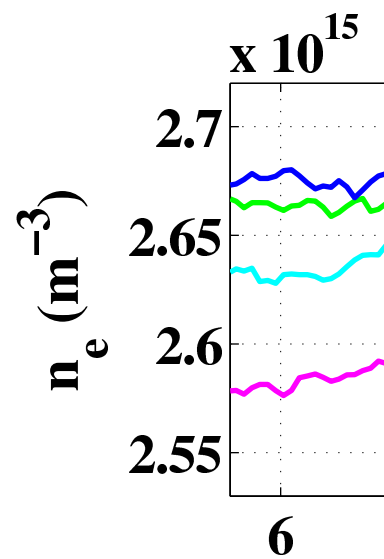
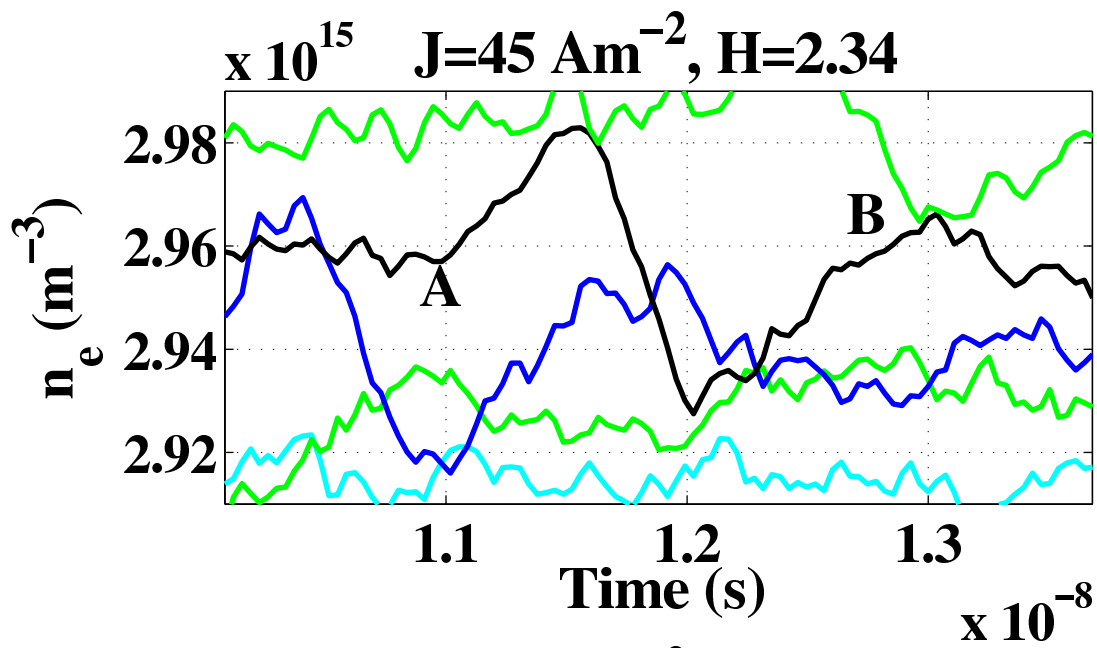


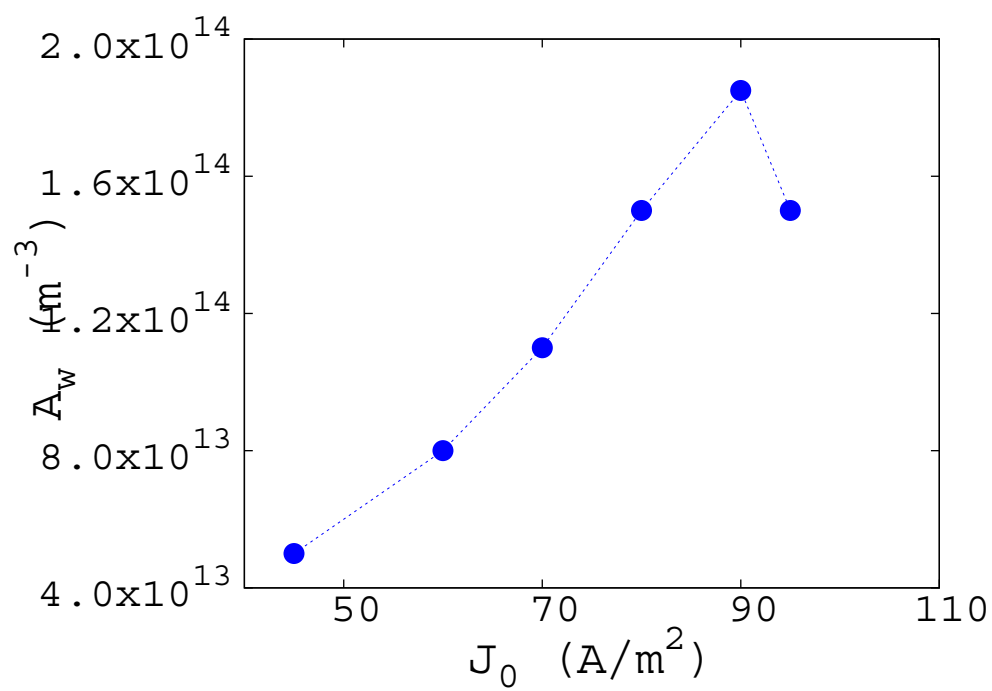
0.03

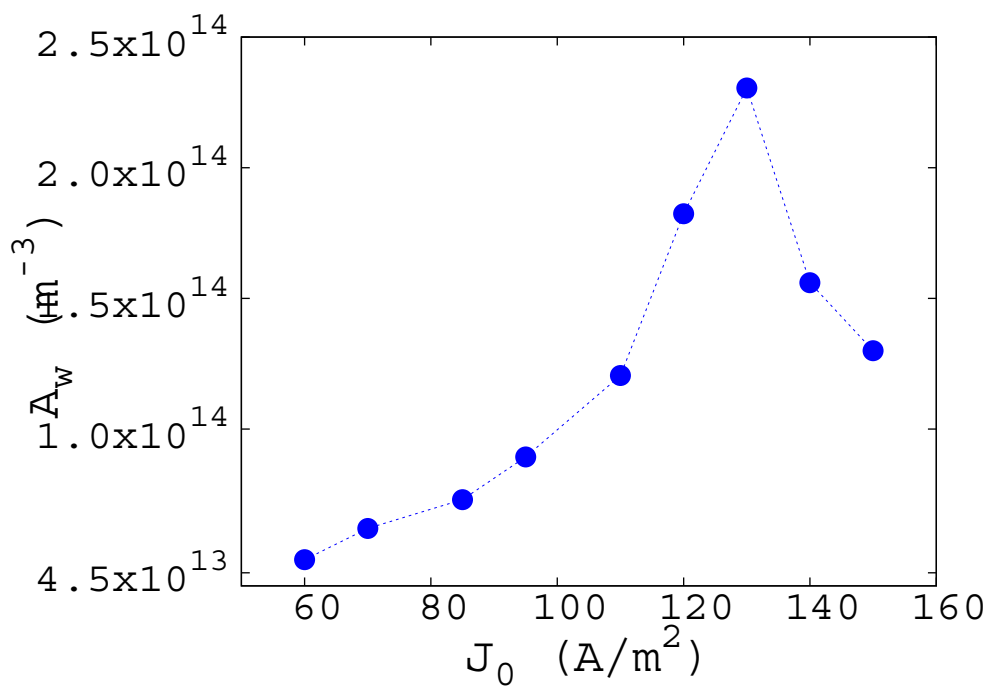
L(m)

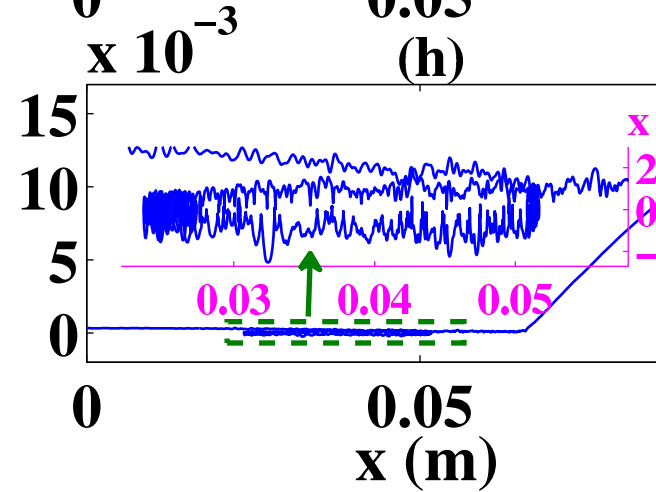
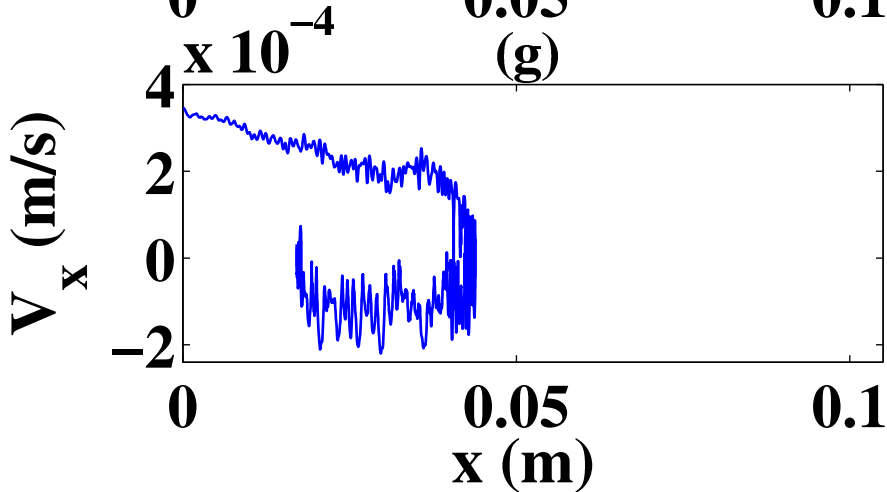
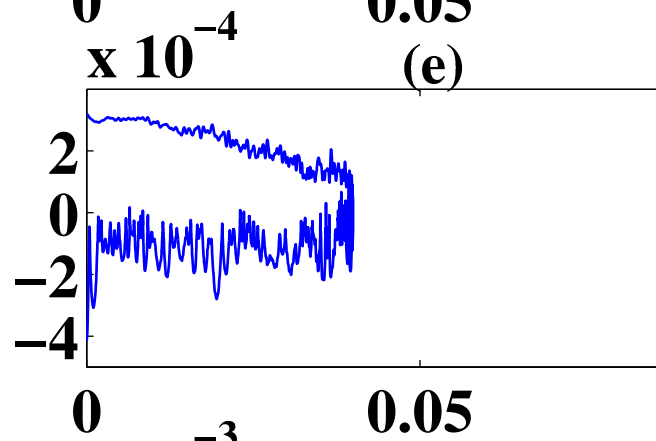
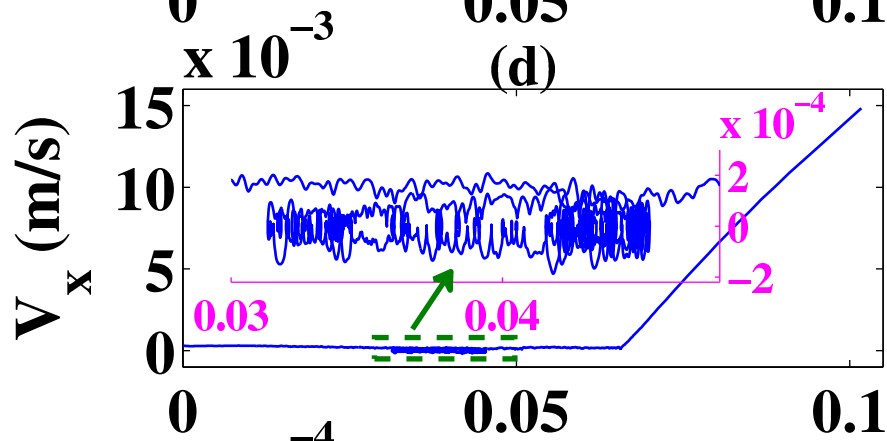
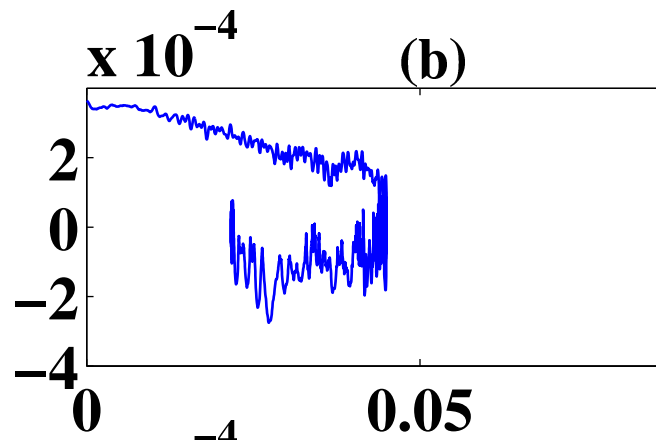
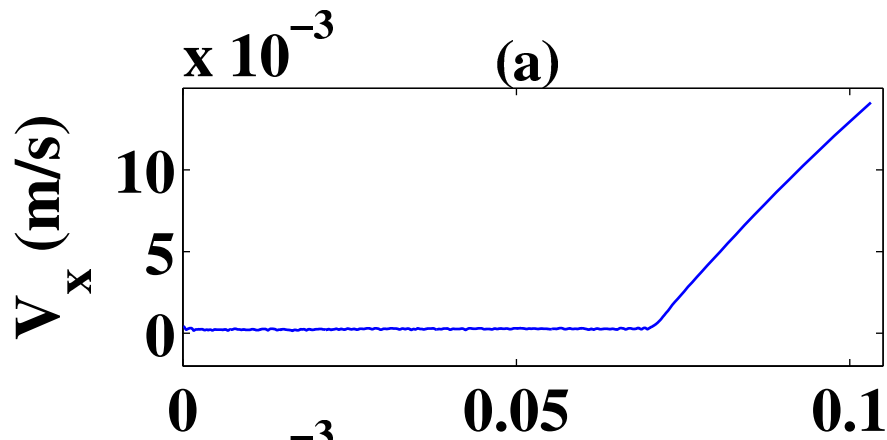


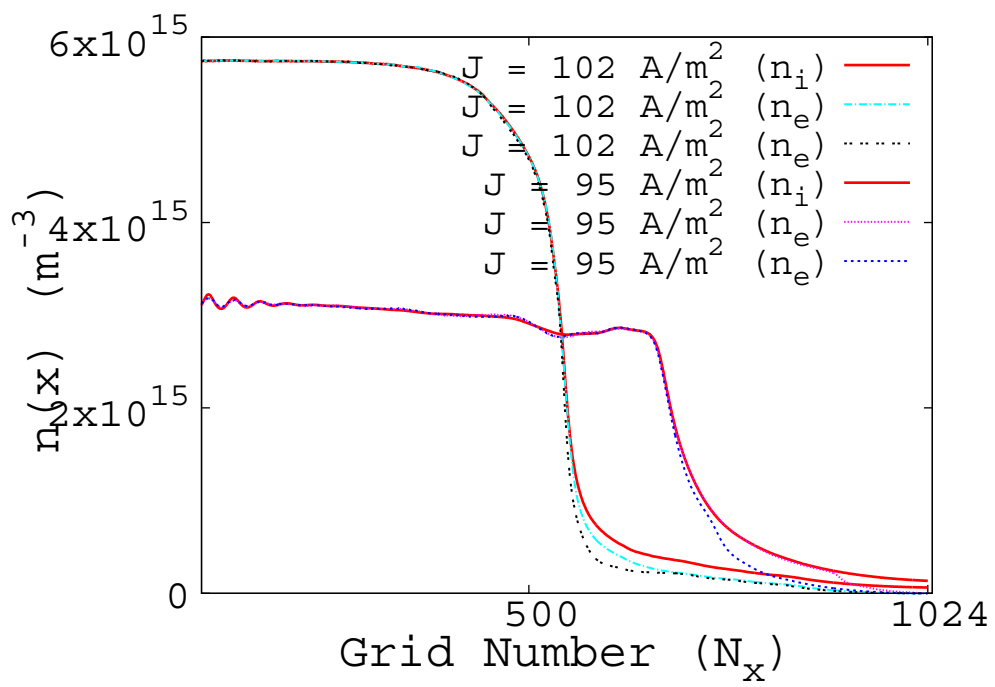












3.6837×10^{-8}

$t(s)$

3

2

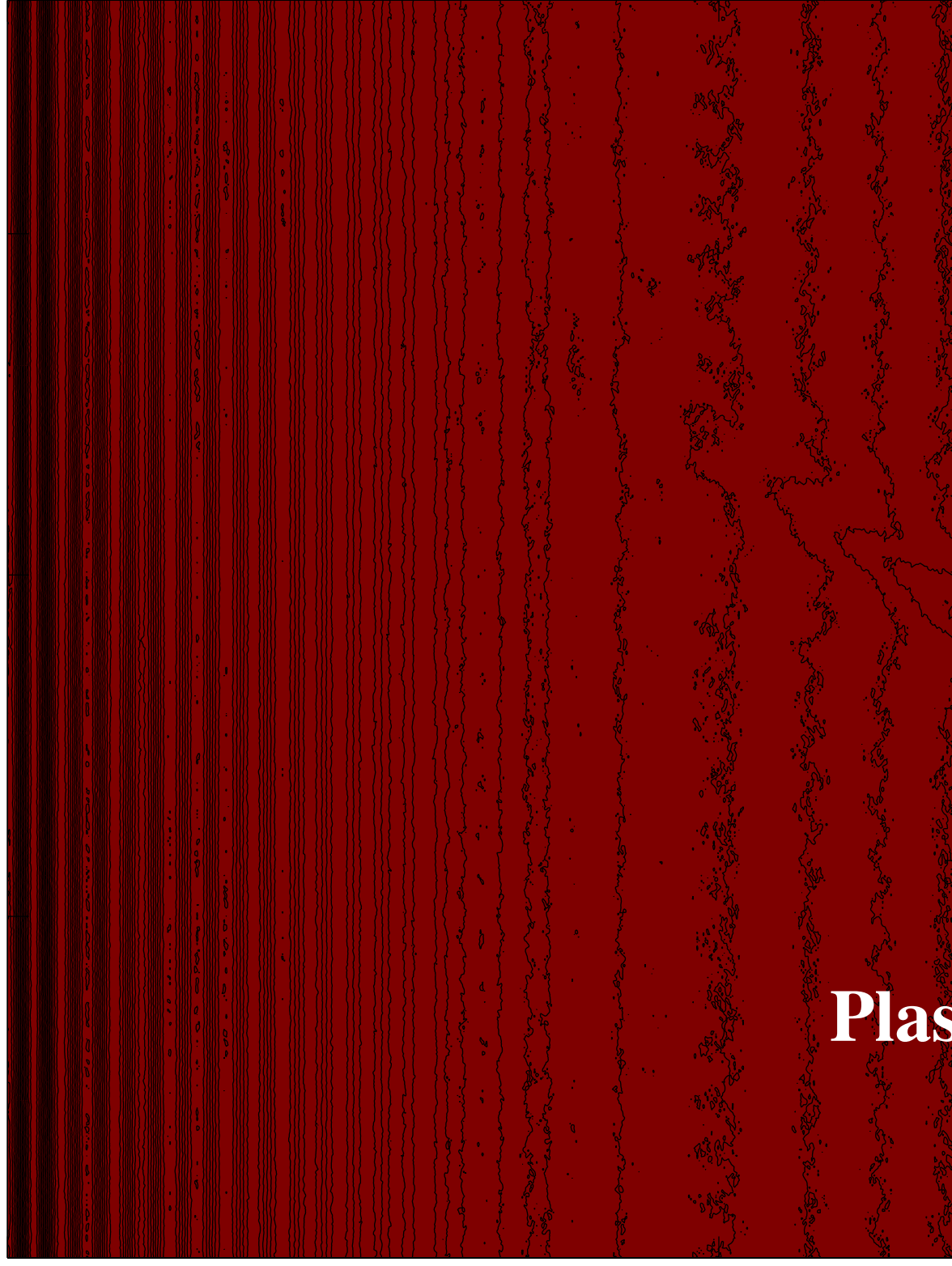
1

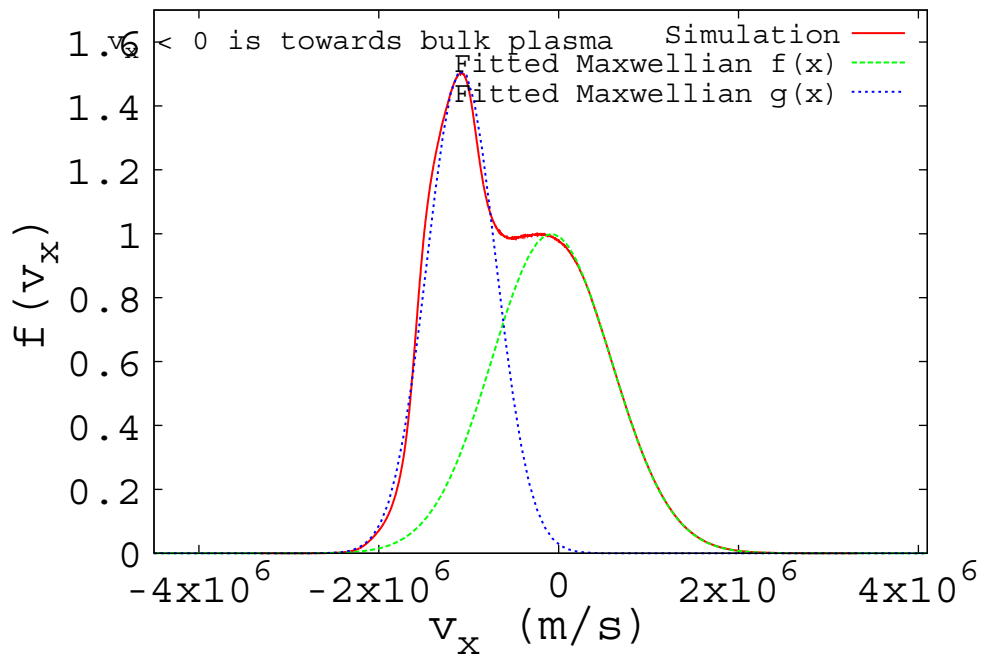
0

0

0.02

Plas





3.6837×10^{-8}

$t(s)$

3

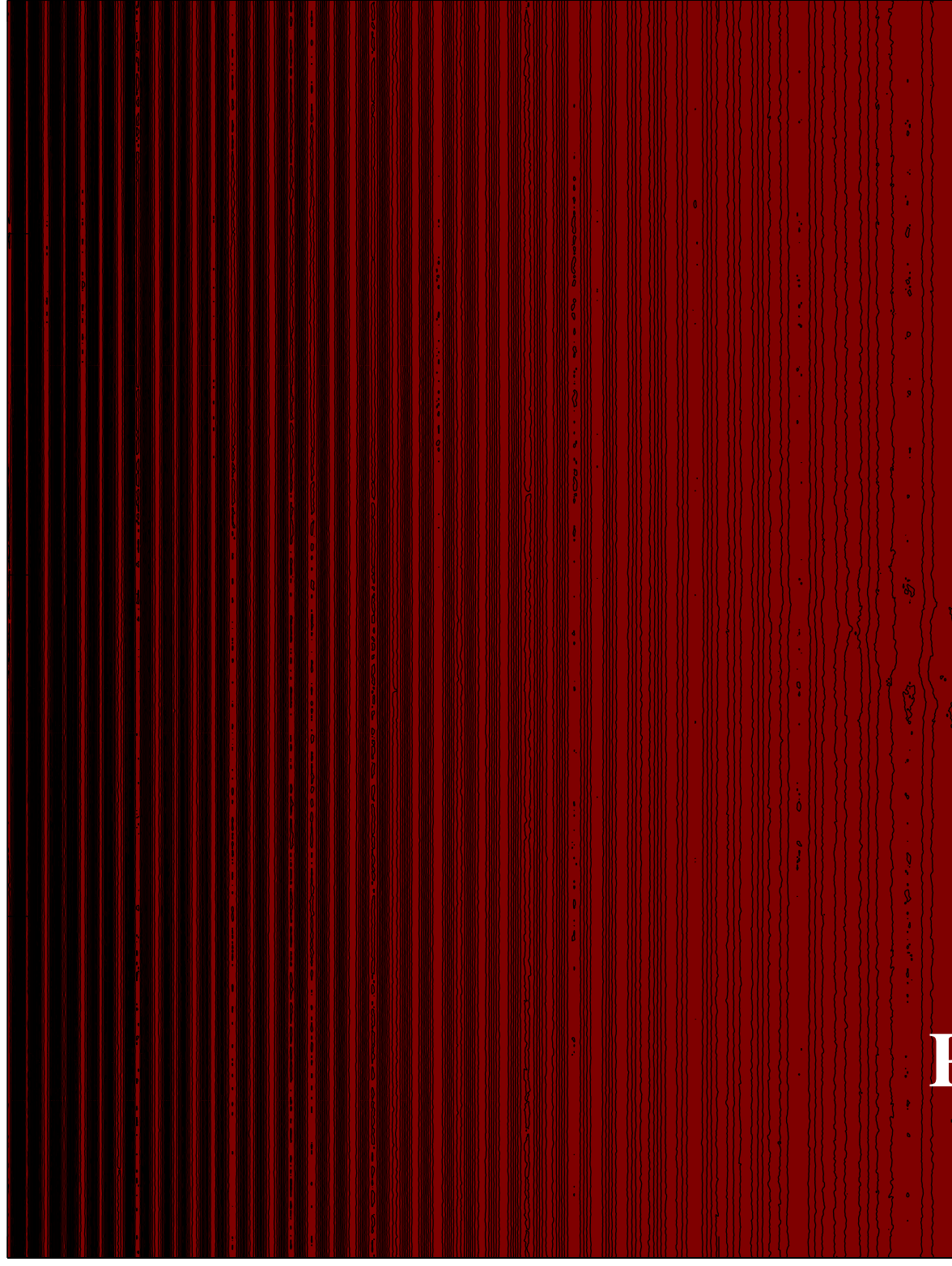
2

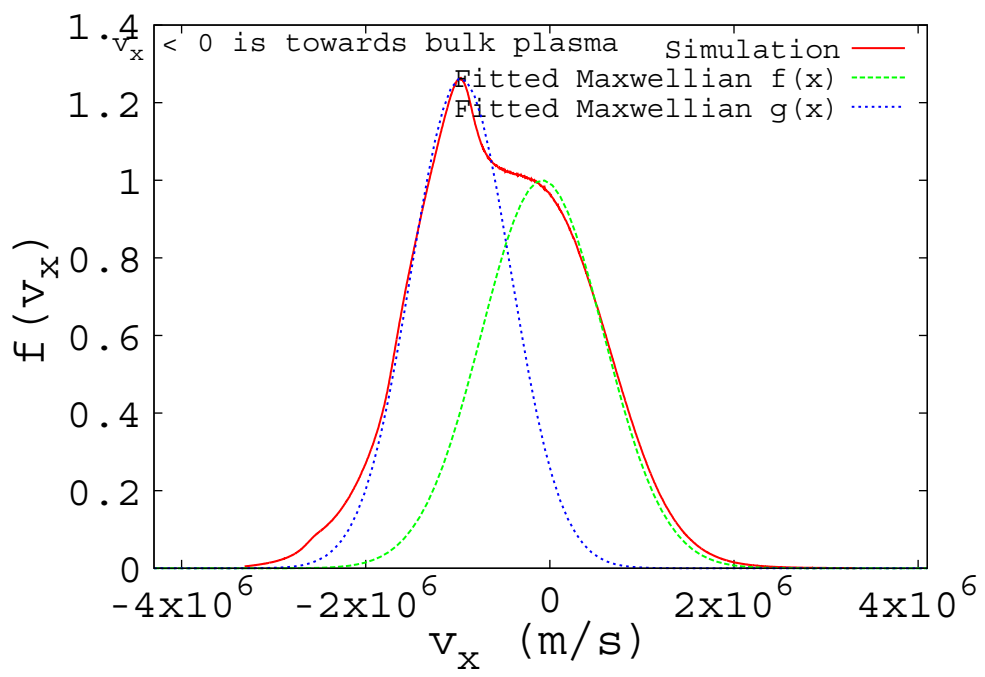
1

0

0

0.02





3.6837×10^{-8}

$t(s)$

3

2

1

0

0

0.02

